

Hybrid Beamforming for mmWave Integrated Sensing and Communication with Multi-static Cooperative Localization

Minghao Yuan, Dongxuan He, *Member, IEEE*, Hao Yin, Hua Wang, *Member, IEEE*,
 Fan Liu, *Senior Member, IEEE*, Zhaocheng Wang, *Fellow, IEEE*, and Tony Q. S. Quek, *Fellow, IEEE*

Abstract—Beamforming is a key technology for achieving integrated sensing and communication (ISAC). However, most existing works focus on mono-static sensing, which has limited sensing accuracy and strong self-interference. To address these issues, this paper investigates hybrid beamforming (HBF) design for millimeter-wave (mmWave) multiple-input multiple-output (MIMO) ISAC system with multi-static cooperative localization. Specifically, one access point (AP) simultaneously forms communication beams to serve multiple user equipments (UEs) and a sensing beam towards one target, and other multiple distributed APs perform cooperative localization on the target by estimating the angle-of-arrivals (AOAs) of received echo signals. First, to characterize the target localization accuracy, we derive the squared position error bound (SPEB) of AOA-based multi-static cooperative localization. Then, two HBF optimization problems are formulated to investigate the performance tradeoff between sensing and communication. For the sensing-centric design, we aim to minimize the SPEB of target localization while ensuring the signal-to-interference-plus-noise ratio (SINR) requirements of individual UEs. To tackle this nonconvex problem, we propose a semidefinite relaxation (SDR)-based alternating optimization algorithm. For the communication-centric design, a fractional programming (FP)-based alternating optimization algorithm is proposed for solving the communication sum-rate maximization problem under the sensing SPEB constraint. Simulation results demonstrate that the proposed two HBF algorithms can achieve localization accuracy and sum-rate performance close to fully-digital beamforming counterparts and outperform other baseline schemes.

Index Terms—Integrated sensing and communication, cooperative localization, squared position error bound, hybrid beamforming, semidefinite relaxation, fractional programming.

This work was supported in part by the National Key Research and Development Program of China under Grant 2024YFE0200404, in part by the National Natural Science Foundation of China under Grant 62101306, in part by the National Natural Science Foundation of China under Grant 62331023, in part by the Guangdong Basic and Applied Basic Research Foundation under Grant 2024A1515011218, and in part by the National Research Foundation, Singapore and Infocomm Media Development Authority under its Future Communications Research & Development Programme. (*Corresponding author: Dongxuan He*.)

Minghao Yuan, Dongxuan He, and Hua Wang are with the School of Information and Electronics, Beijing Institute of Technology, Beijing 100081, China (e-mail: minghaoyuan@bit.edu.cn; dongxuan_he@bit.edu.cn; wanghua@bit.edu.cn).

Hao Yin is with Institute of China Electronic System Engineering, Beijing 100141, China (e-mail: yinhao@cashq.ac.cn).

Fan Liu is with the National Mobile Communications Research Laboratory, Southeast University, Nanjing 210096, China (e-mail: f.liu@ieee.org).

Zhaocheng Wang is with Beijing National Research Center for Information Science and Technology, Department of Electronic Engineering, Tsinghua University, Beijing 100084, China (e-mail: zcwang@tsinghua.edu.cn).

Tony Q. S. Quek is with the Information Systems Technology and Design Pillar, Singapore University of Technology and Design, Singapore 487372 (e-mail: tonyquek@sutd.edu.sg).

I. INTRODUCTION

Future wireless networks are envisioned to have high-quality communication and high-accuracy sensing capabilities for enabling various emerging applications, such as smart manufacturing, vehicle-to-everything, and low-altitude economy [1]. Meanwhile, both sensing and communication systems are developing towards high frequency bands, large bandwidth, and large-scale antenna arrays, thereby having increasing similarities in transceiver architectures and signal processing techniques [1]–[3]. The above factors have motivated the joint design of sensing and communication systems. Integrated sensing and communication (ISAC) is expected to achieve dual functionalities of radar sensing and wireless communication simultaneously by using the same spectrum resource and hardware platform, thus improving spectral efficiency while reducing hardware cost [4]. In recent years, ISAC has been widely considered as a key enabling technology for the sixth generation (6G) wireless networks [1], [5]. Extensive research efforts in terms of fundamental theory [4], [6], waveform design [7], [8], and beamforming design [9] have been conducted to promote the development of ISAC technology.

A. Related Works

Exploiting the spatial degrees of freedom provided by multi-antenna technology, beamforming can realize high-data rate communication and high-accuracy target sensing simultaneously [10], [11]. In recent years, beamforming design for multiple-input multiple-output (MIMO) ISAC systems has been extensively investigated [10]–[13]. Specifically, several optimization-based beamforming designs were proposed for multiuser ISAC systems to approximate the sensing-only beampattern, while satisfying the signal-to-interference-plus-noise ratio (SINR) requirements of individual communication user equipments (UEs) [10]. Compared to [10], the beamforming design in [11] provided extra degrees of freedom by introducing the dedicated sensing waveform, thus improving the transmit beampattern performance. In [12], the achievable performance region of MIMO ISAC systems was defined and two beamforming approaches were proposed to achieve the performance tradeoff between sensing SINR and communication sum-rate. Different from using the beampattern [10], [11] and SINR [12] as sensing metrics, the Cramér-Rao bound (CRB) was adopted to characterize the performance of target angle estimation and formulate the beamforming optimization problem [13].

TABLE I
A COMPARISON OF THE RELATED LITERATURE WITH OUR WORK

Sensing type	Reference	System model	Frequency band	ISAC approach	Sensing metric	Comm. metric
Mono-static	[10]	Single-BS MIMO ISAC	Sub-6GHz	FDBF	Beampattern	SINR
	[11]	Single-BS MIMO ISAC	Sub-6GHz	FDBF	Beampattern	SINR
	[12]	Single-BS MIMO ISAC	Sub-6GHz	FDBF	SINR	Sum-rate
	[13]	Single-BS MIMO ISAC	Sub-6GHz	FDBF	CRB for AOA estimation	SINR
	[18]	Single-BS MIMO ISAC	MmWave	HBF	Beampattern	Rate
	[19]	Single-BS MIMO ISAC	MmWave	HBF	CRB for AOA estimation	SINR
Multi-static	[22]	Networked MIMO ISAC	Sub-6GHz	FDBF	Detection probability	SINR
	[23]	Multi-AP MIMO ISAC	Sub-6GHz	FDBF	Detection probability	SINR
	[24]	Cell-free massive MIMO ISAC	Sub-6GHz	FDBF	Beampattern	Sum-rate
	[25]	Networked single-antenna ISAC	Sub-6GHz	Power control	TOA-based SPEB	SINR
	Our work	Multi-AP MIMO ISAC	MmWave	HBF	AOA-based SPEB	SINR, Sum-rate

However, the aforementioned works [10]–[13] focus on MIMO ISAC systems operating in lower frequency bands such as sub-6GHz, which are typically implemented by fully-digital beamforming (FDBF). This architecture is infeasible for millimeter-wave (mmWave) systems equipped with massive antennas due to high hardware cost and power consumption. Compared to FDBF, hybrid beamforming (HBF) is capable of significantly reducing the number of radio frequency (RF) chains while maintaining high beamforming gain, thus striking a balance between system performance and hardware complexity [14]–[16]. In recent years, HBF design for mmWave ISAC systems has attracted considerable research interest [9], [17]–[19]. For instance, a communication quality-of-service (QoS) aware HBF approach was designed to minimize the beampattern matching error [18]. Nevertheless, the work [18] considered the HBF with fully-connected architecture, which still had high hardware complexity due to massive phase shifters. To further reduce hardware complexity, a partially-connected architecture-based HBF scheme was proposed to minimize the CRB of angle estimation under communication SINR requirements [19].

Despite the extensive research progress, existing works mainly focus on mono-static sensing, whose sensing accuracy and range are limited. To break through the bottleneck of mono-static sensing, exploiting multiple base stations (BSs) in cellular networks for multi-static cooperative sensing has been considered as a promising solution [20], [21]. On the one hand, multi-static cooperative sensing can provide spatial diversity gains through multi-angle observations, thus enhancing sensing accuracy. On the other hand, multi-static cooperative sensing can expand coverage range and achieve seamless sensing. Recently, multi-static cooperative ISAC systems have received growing attention [22]–[24]. For instance, a networked MIMO ISAC system was studied in [22], where the coordinated transmit beamforming of multiple BSs was designed to achieve multicell communication and distributed target detection. In [23], a power optimization algorithm based on cooperative active and passive sensing was proposed to improve the target detection performance. In addition, the transmit beamforming designs for cell-free massive MIMO ISAC systems were investigated to achieve the performance

tradeoff between sensing beampattern matching error and communication sum-rate [24].

Although the target detection [22], [23] and beampattern design [24] have been studied, there is almost no work on beamforming design for enhancing the target localization accuracy in multi-static cooperative ISAC systems. In particular, the power control of a networked ISAC system was designed to achieve the transmit power minimization under communication QoS and target localization accuracy constraints [25]. Nevertheless, it is assumed in [25] that all the BSs are equipped with single-antenna, which cannot exploit the spatial degrees of freedom provided by multi-antenna to mitigate multiuser interference and improve localization accuracy. The aforementioned related works are summarized in Table I. To the best of our knowledge, beamforming design for multi-static cooperative MIMO ISAC system considering target localization has not been investigated yet, it is still a significant and open problem. Also, the tradeoff between localization accuracy and communication performance in this system needs to be explored.

B. Contributions

This paper investigates HBF design for mmWave MIMO ISAC systems with multi-static cooperative localization. The main contributions of this paper are summarized as follows:

- We propose a multi-static mmWave MIMO ISAC system for achieving multiuser communication and target localization simultaneously. In this system, one access point (AP) acts as the ISAC transmitter to form multiple communication beams to serve a set of UEs and one sensing beam towards one target, and other multiple distributed APs act as the sensing receivers to cooperatively locate on the target by estimating the angle-of-arrivals (AOAs) of echo signals. On the one hand, compared to the colocated MIMO systems [10]–[13], [17]–[19] and single-antenna system [25], the proposed system can significantly enhance the target localization accuracy by simultaneously leveraging the spatial degrees of freedom and spatial diversity gains provided by distributed MIMO. On the other hand, compared to the ISAC systems with mono-static sensing [10]–[13], [17]–[19], the proposed ISAC

system with multi-static cooperative passive sensing can effectively overcome self-interference issue.

- To characterize the target localization accuracy, we derive the squared position error bound (SPEB) of AOA-based multi-static cooperative localization by utilizing the equivalent Fisher information matrix (EFIM). Different from adopting the CRB as the performance metric of target AOA estimation [13], [19], we exploit the SPEB to intuitively characterize the target localization accuracy. On this basis, to investigate the performance tradeoff between sensing and communication, we formulate two HBF optimization problems consisting of sensing-centric design and communication-centric design.
- For the sensing-centric design, we aim to optimize the HBF to minimize the SPEB of target localization, while satisfying the SINR requirements of individual communication UEs. This intractable problem is first reformulated as a tractable form by exploiting matrix-monotonic optimization and Schur complement. Then, the resulting problem is decoupled based on alternating optimization framework. The digital beamformer and analog beamformer are designed by leveraging the semidefinite relaxation (SDR) technique.
- For the communication-centric design, the HBF optimization is formulated as the communication sum-rate maximization problem under the SPEB constraint of target localization. To tackle the nonconvex problem, we propose an alternating optimization algorithm based on fractional programming (FP) and convex relaxation techniques.
- Simulation results demonstrate that the proposed sensing-centric HBF design achieves target localization accuracy close to the FDBF counterpart and outperforms other baseline schemes, and the proposed communication-centric HBF design achieves significant sum-rate performance improvement compared to the existing approach.

The remainder of this paper is organized as follows. Section II presents the system model. Section III derives the SPEB of target localization and formulates two HBF optimization problems. Section IV proposes a sensing-centric HBF design. Section V proposes a communication-centric HBF design. Section VI presents sensing-centric and communication-centric FDBF designs. Section VII provides numerical results. Finally, Section VIII concludes this paper.

Notations: Boldface lowercase and uppercase letters represent vectors and matrices, respectively. $\mathbb{C}^{M \times N}$ and $\mathbb{R}^{M \times N}$ denote the spaces of $M \times N$ complex and real matrices, respectively. $\mathbb{E}\{\cdot\}$ represents the statistical expectation. $(\cdot)^*$, $(\cdot)^T$, and $(\cdot)^H$ represent the conjugate, transpose, and conjugate transpose, respectively. $(\cdot)^{-1}$, $\text{tr}(\cdot)$, and $\text{rank}(\cdot)$ represent the inversion, trace, and rank of a matrix, respectively. $[\mathbf{x}]_j$ represents the j -th element of vector \mathbf{x} . $[\mathbf{X}]_{i,j}$ represents the (i,j) -th element of matrix \mathbf{X} . $\text{diag}(\cdot)$ and $\text{blkdiag}\{\cdot\}$ denote the operations of diagonalization and block diagonalization, respectively. $\mathcal{CN}(\mu, \Sigma)$ denotes the complex Gaussian distribution with mean μ and covariance matrix Σ . \mathbf{I}_N represents an $N \times N$ identity matrix. $|\cdot|$ denotes the absolute value of

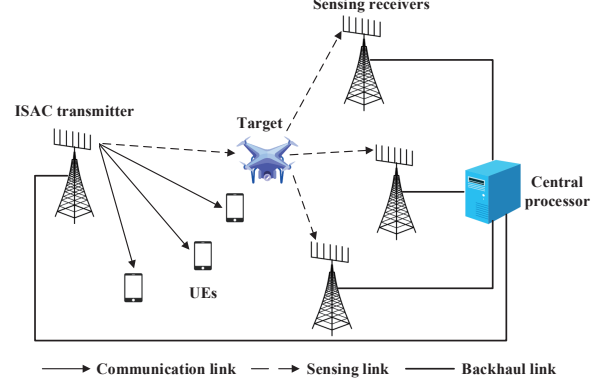


Fig. 1. A multi-static mmWave MIMO ISAC system.

a scalar. $\|\cdot\|_F$ denotes the Frobenius norm of a matrix. $\text{Re}\{\cdot\}$ and $\text{Im}\{\cdot\}$ denote the real and imaginary parts of a complex number, respectively.

II. SYSTEM MODEL

We consider a multi-static mmWave MIMO ISAC system consisting of $M+1$ distributed APs, where one AP acts as the ISAC transmitter, the other M APs act as the sensing receivers [23], [26]. All the APs are connected to a central processor via backhaul links for information exchange and are assumed to be synchronized [22], [23]. As depicted in Fig. 1, the ISAC transmitter equipped with N_t antennas simultaneously forms communication beams to serve K single-antenna UEs and one sensing beam towards one target, and then the M sensing receivers equipped with N_r antennas receive the echo signals reflected by the target. In this system, we consider cooperative passive sensing and data-level fusion [21], which can overcome self-interference and reduce signaling overhead. Specifically, the M sensing receivers first estimate the individual AOAs of received echo signals in a distributed manner and then transmit the sensing results to the central processor for performing the cooperative localization on the target¹. The above processing is completed in a coherent processing interval (CPI) [27], thus channel parameters and target parameters are assumed to be unchanged. Without loss of generality, all the APs are equipped with uniform linear arrays (ULAs). To reduce the hardware complexity, we adopt the partially-connected HBF architecture [17], [19]. Specifically, the ISAC transmitter is equipped with N_{RF} RF chains, each of which is connected to a subarray with N_t/N_{RF} antennas via phase shifters.

¹The acquisition of target position consists of two stages. During the first stage, the transmitter radiates omnidirectional signal by using single-antenna, and multiple sensing receivers respectively estimate the AOAs of echo signals reflected by the target, which are then transmitted to the central processor for calculating the initial estimate of target position. However, the target localization accuracy during the first stage is limited. During the second stage, by exploiting the initial estimate of target position, the transmitter equipped with multi-antenna forms directional high-gain beam towards the target through HBF design, thus further improving the target localization accuracy. In this paper, we mainly focus on the HBF design during the second stage.

A. Communication Model

We focus on the HBF architecture-based downlink multiuser communication. Let $\mathbf{s}(t) = [s_1(t), \dots, s_K(t)]^T \in \mathbb{C}^{K \times 1}$ denote the transmitted data symbol vector for K communication UEs at the time instant t , which satisfies $\mathbb{E}\{\mathbf{s}(t)\mathbf{s}^H(t)\} = \mathbf{I}_K$. After HBF processing, the transmit signal of the ISAC transmitter is expressed as

$$\mathbf{x}(t) = \mathbf{F}_{\text{RF}} \mathbf{F}_{\text{BBS}}(t) = \mathbf{F}_{\text{RF}} \sum_{k=1}^K \mathbf{f}_{\text{BB},k} s_k(t), \quad (1)$$

where $\mathbf{F}_{\text{BB}} = [\mathbf{f}_{\text{BB},1}, \dots, \mathbf{f}_{\text{BB},K}] \in \mathbb{C}^{N_{\text{RF}} \times K}$ represents the digital beamformer, and $\mathbf{F}_{\text{RF}} \in \mathbb{C}^{N_t \times N_{\text{RF}}}$ represents the partially-connected analog beamformer with block diagonal structure, which is represented as

$$\mathbf{F}_{\text{RF}} = \text{blkdiag}\{\mathbf{f}_1, \dots, \mathbf{f}_{N_{\text{RF}}}\}, \quad (2)$$

where $\mathbf{f}_i \in \mathbb{C}^{\frac{N_t}{N_{\text{RF}}} \times 1}$ is a vector with each element satisfying the unit modulus constraint, i.e., $|\mathbf{f}_i|_j = 1, j = 1, \dots, N_t/N_{\text{RF}}$.

The received signal of the k -th communication UE is expressed as

$$y_k(t) = \mathbf{h}_k^H \mathbf{F}_{\text{RF}} \mathbf{f}_{\text{BB},k} s_k(t) + \sum_{j=1, j \neq k}^K \mathbf{h}_k^H \mathbf{F}_{\text{RF}} \mathbf{f}_{\text{BB},j} s_j(t) + z_k(t), \quad (3)$$

where $\mathbf{h}_k \in \mathbb{C}^{N_t \times 1}$ represents the mmWave channel vector, and $z_k(t) \sim \mathcal{CN}(0, \sigma_n^2)$ represents the Gaussian noise with σ_n^2 being noise power.

Adopting the Saleh-Valenzuela model [9], [17]–[19], the mmWave channel vector between the ISAC transmitter and the k -th communication UE is expressed as

$$\mathbf{h}_k = \sum_{l=1}^{L_k} \beta_{k,l} \mathbf{a}_t(\phi_{k,l}), \quad (4)$$

where L_k denotes the number of propagation paths, $\beta_{k,l}$ denotes the complex gain considering large-scale fading of the l -th path, $\phi_{k,l}$ denotes the angle-of-departure (AOD) of the l -th path, and the transmit array response vector $\mathbf{a}_t(\phi_{k,l})$ is represented as

$$\mathbf{a}_t(\phi_{k,l}) = \left[1, e^{j \frac{2\pi d}{\lambda} \sin \phi_{k,l}}, \dots, e^{j(N_t-1) \frac{2\pi d}{\lambda} \sin \phi_{k,l}} \right]^T, \quad (5)$$

where λ denotes the carrier wavelength, and d denotes the spacing between adjacent antennas.

It is assumed that perfect channel state information is available at the ISAC transmitter. Therefore, the SINR of the k -th communication UE is represented as

$$\text{SINR}_k = \frac{|\mathbf{h}_k^H \mathbf{F}_{\text{RF}} \mathbf{f}_{\text{BB},k}|^2}{\sum_{j=1, j \neq k}^K |\mathbf{h}_k^H \mathbf{F}_{\text{RF}} \mathbf{f}_{\text{BB},j}|^2 + \sigma_n^2}. \quad (6)$$

B. Sensing Model

For the target sensing, we assume that the line-of-sight (LOS) path between each AP and the target exists [22]–

[28]. Therefore, at the t -th snapshot, the received echo signal $\mathbf{y}_m(t) \in \mathbb{C}^{N_r \times 1}$ of the m -th sensing receiver is expressed as

$$\begin{aligned} \mathbf{y}_m(t) &= \alpha_m \mathbf{A}_m \mathbf{x}(t) + \mathbf{n}_m(t) \\ &= \alpha_m \mathbf{a}_r(\theta_m) \mathbf{a}_t^H(\theta_0) \mathbf{x}(t) + \mathbf{n}_m(t), \end{aligned} \quad (7)$$

where α_m denotes the reflection coefficient consisting of both the distance-dependent path loss and the radar cross section (RCS) of the target, $\mathbf{n}_m(t) \sim \mathcal{CN}(0, \sigma_n^2 \mathbf{I}_{N_r})$ denotes the Gaussian noise vector, θ_0 represents the AOD of the target with respect to (w.r.t.) the ISAC transmitter, θ_m represents the AOA of the target w.r.t. the m -th sensing receiver, and the transmit and receive array response vectors are respectively represented as

$$\mathbf{a}_t(\theta_0) = \left[1, e^{j \frac{2\pi d}{\lambda} \sin \theta_0}, \dots, e^{j(N_t-1) \frac{2\pi d}{\lambda} \sin \theta_0} \right]^T, \quad (8a)$$

$$\mathbf{a}_r(\theta_m) = \left[1, e^{j \frac{2\pi d}{\lambda} \sin \theta_m}, \dots, e^{j(N_r-1) \frac{2\pi d}{\lambda} \sin \theta_m} \right]^T. \quad (8b)$$

According to (7), the received echo signal over T snapshots during a coherent time block at the m -th sensing receiver is expressed as

$$\mathbf{Y}_m = \alpha_m \mathbf{a}_r(\theta_m) \mathbf{a}_t^H(\theta_0) \mathbf{X} + \mathbf{N}_m, \quad (9)$$

where $\mathbf{Y}_m = [\mathbf{y}_m(1), \dots, \mathbf{y}_m(T)]$, $\mathbf{X} = [\mathbf{x}(1), \dots, \mathbf{x}(T)]$, $\mathbf{N}_m = [\mathbf{n}_m(1), \dots, \mathbf{n}_m(T)]$. The covariance matrix of transmit signal is represented as

$$\begin{aligned} \mathbf{R}_X &= \frac{1}{T} \mathbf{X} \mathbf{X}^H = \frac{1}{T} \mathbf{F}_{\text{RF}} \mathbf{F}_{\text{BB}} \mathbf{S} \mathbf{S}^H \mathbf{F}_{\text{BB}}^H \mathbf{F}_{\text{RF}}^H \\ &\approx \mathbf{F}_{\text{RF}} \mathbf{F}_{\text{BB}} \mathbf{F}_{\text{BB}}^H \mathbf{F}_{\text{RF}}^H. \end{aligned} \quad (10)$$

where the approximation tends to be accurate when T is sufficiently large [13].

III. SPEB ANALYSIS AND PROBLEM FORMULATION

A. SPEB Analysis of AOA-based Cooperative Localization

The target localization accuracy is typically characterized by the SPEB [29], [30], i.e., the CRB for position estimation. Different from adopting the CRB as the performance metric of target angle estimation [13], [19], in this paper, we exploit the SPEB of AOA-based cooperative localization to intuitively characterize the target localization accuracy. In this subsection, we first analyze the equivalent Fisher information matrix (EFIM) of all the AOAs, and then transform it into the SPEB of target localization.

In (9), the AOD θ_0 is typically known to the ISAC transmitter since it can be acquired from previous observations [11]. For the m -th sensing receiver, let $\xi_m = [\theta_m, \tilde{\alpha}_m^T]^T \in \mathbb{R}^{3 \times 1}$ denote the vector composed of unknown parameters, where θ_m is the parameter of interest, $\tilde{\alpha}_m = [\text{Re}\{\alpha_m\}, \text{Im}\{\alpha_m\}]^T$ is the nuisance parameter vector. The received echo signal in (9) can be vectorized as

$$\tilde{\mathbf{y}}_m = \text{vec}(\mathbf{Y}_m) = \boldsymbol{\eta}_m + \tilde{\mathbf{n}}_s, \quad (11)$$

where $\boldsymbol{\eta}_m = \alpha_m \text{vec}(\mathbf{A}_m \mathbf{X}) \in \mathbb{C}^{N_r T \times 1}$ and $\tilde{\mathbf{n}}_s = \text{vec}(\mathbf{N}_m) \in \mathbb{C}^{N_r T \times 1}$.

$$J_{\theta_m \theta_m}^e = J_{\theta_m \theta_m} - \mathbf{J}_{\theta_m \tilde{\alpha}_m} \mathbf{J}_{\tilde{\alpha}_m \tilde{\alpha}_m}^{-1} \mathbf{J}_{\theta_m \tilde{\alpha}_m}^T \quad (14a)$$

$$= \frac{2T|\alpha_m|^2}{\sigma_n^2} \left(\text{tr}(\dot{\mathbf{A}}_m \mathbf{F}_{\text{RF}} \mathbf{F}_{\text{BB}} \mathbf{F}_{\text{BB}}^H \mathbf{F}_{\text{RF}}^H \dot{\mathbf{A}}_m^H) - \frac{|\text{tr}(\mathbf{A}_m \mathbf{F}_{\text{RF}} \mathbf{F}_{\text{BB}} \mathbf{F}_{\text{BB}}^H \mathbf{F}_{\text{RF}}^H \dot{\mathbf{A}}_m^H)|^2}{\text{tr}(\mathbf{A}_m \mathbf{F}_{\text{RF}} \mathbf{F}_{\text{BB}} \mathbf{F}_{\text{BB}}^H \mathbf{F}_{\text{RF}}^H \mathbf{A}_m^H)} \right) \quad (14b)$$

$$= \frac{2T|\alpha_m|^2}{\sigma_n^2} \left(\text{tr}(\dot{\mathbf{A}}_m \mathbf{R}_X \dot{\mathbf{A}}_m^H) - \frac{|\text{tr}(\mathbf{A}_m \mathbf{R}_X \dot{\mathbf{A}}_m^H)|^2}{\text{tr}(\mathbf{A}_m \mathbf{R}_X \mathbf{A}_m^H)} \right). \quad (14c)$$

According to [31], the Fisher information matrix (FIM) for estimating ξ_m from the sufficient statistic $\tilde{\mathbf{y}}_m$ can be partitioned as

$$\mathbf{J}(\xi_m) = \begin{bmatrix} J_{\theta_m \theta_m} & \mathbf{J}_{\theta_m \tilde{\alpha}_m} \\ \mathbf{J}_{\theta_m \tilde{\alpha}_m}^T & \mathbf{J}_{\tilde{\alpha}_m \tilde{\alpha}_m} \end{bmatrix} \in \mathbb{R}^{3 \times 3}, \quad (12)$$

where

$$J_{\theta_m \theta_m} = \frac{2T|\alpha_m|^2}{\sigma_n^2} \text{tr}(\dot{\mathbf{A}}_m \mathbf{F}_{\text{RF}} \mathbf{F}_{\text{BB}} \mathbf{F}_{\text{BB}}^H \mathbf{F}_{\text{RF}}^H \dot{\mathbf{A}}_m^H), \quad (13a)$$

$$\mathbf{J}_{\theta_m \tilde{\alpha}_m} = \frac{2T}{\sigma_n^2} \text{Re} \left\{ \alpha_m^* \text{tr}(\mathbf{A}_m \mathbf{F}_{\text{RF}} \mathbf{F}_{\text{BB}} \mathbf{F}_{\text{BB}}^H \mathbf{F}_{\text{RF}}^H \dot{\mathbf{A}}_m^H)[1, j] \right\} \in \mathbb{R}^{1 \times 2}, \quad (13b)$$

$$\mathbf{J}_{\tilde{\alpha}_m \tilde{\alpha}_m} = \frac{2T}{\sigma_n^2} \text{tr}(\mathbf{A}_m \mathbf{F}_{\text{RF}} \mathbf{F}_{\text{BB}} \mathbf{F}_{\text{BB}}^H \mathbf{F}_{\text{RF}}^H \mathbf{A}_m^H) \mathbf{I}_2 \in \mathbb{R}^{2 \times 2}, \quad (13c)$$

and $\dot{\mathbf{A}}_m = \frac{\partial \mathbf{A}_m}{\partial \theta_m}$ represents the partial derivative of \mathbf{A}_m w.r.t. θ_m .

The SPEB is derived by utilizing the equivalent Fisher information (EFI) [29], which is defined as a measure of the information related to the parameters of interest by considering the uncertainties of the nuisance parameters [30]. By isolating the impact of the nuisance parameter vector $\tilde{\alpha}_m$, the EFI of θ_m can be given by (14) at the top of this page.

Notice that the EFI $J_{\theta_m \theta_m}^e$ retains all the necessary information to derive the information inequality for θ_m [29].

Therefore, the CRB for estimating θ_m can be given by

$$\text{CRB}(\theta_m) = [J_{\theta_m \theta_m}^e]^{-1}. \quad (15)$$

In this system, the parameters of interest are all the AOAs, which are defined as $\boldsymbol{\theta} = [\theta_1, \dots, \theta_M]^T$. Note that the AOAs of the target relative to different sensing receivers are independent, the EFIM of all the AOAs $\boldsymbol{\theta}$ can be expressed as

$$\mathbf{J}(\boldsymbol{\theta}) = \text{diag}(J_{\theta_1 \theta_1}^e, \dots, J_{\theta_M \theta_M}^e). \quad (16)$$

Next, we analyze the SPEB of AOA-based multi-static cooperative localization. Let $\mathbf{p} = [x, y]^T$ represent the position of the target, and $\mathbf{p}_m = [x_m, y_m]^T$ represent the position of the m -th sensing receiver. It is assumed that the positions of all sensing receivers are known. The geometric relationship between the position of target and the AOA of target echo signal can be represented as

$$\theta_m = \arctan \frac{y - y_m}{x - x_m}. \quad (17)$$

The partial derivatives $\frac{\partial \theta_m}{\partial x}$ and $\frac{\partial \theta_m}{\partial y}$ are respectively given by

$$\frac{\partial \theta_m}{\partial x} = \frac{y_m - y}{(x - x_m)^2 + (y - y_m)^2}, \quad (18a)$$

$$\frac{\partial \theta_m}{\partial y} = \frac{x - x_m}{(x - x_m)^2 + (y - y_m)^2}. \quad (18b)$$

The FIM of AOA-based multi-static cooperative localization can be represented as

$$\mathbf{J}(\mathbf{p}) = \mathbf{V} \mathbf{J}(\boldsymbol{\theta}) \mathbf{V}^T = \sum_{m=1}^M \mathbf{v}_m J_{\theta_m \theta_m}^e \mathbf{v}_m^T, \quad (19)$$

where the Jacobian matrix \mathbf{V} can be given by

$$\mathbf{V} = \frac{\partial \boldsymbol{\theta}^T}{\partial \mathbf{p}} = \begin{bmatrix} \frac{\partial \theta_1}{\partial x} & \dots & \frac{\partial \theta_M}{\partial x} \\ \frac{\partial \theta_1}{\partial y} & \dots & \frac{\partial \theta_M}{\partial y} \end{bmatrix}, \quad (20)$$

and $\mathbf{v}_m = \frac{\partial \theta_m}{\partial \mathbf{p}} = \left[\frac{\partial \theta_m}{\partial x}, \frac{\partial \theta_m}{\partial y} \right]^T$ is the m -th column of \mathbf{V} . The SPEB of AOA-based cooperative localization can be represented as

$$\text{SPEB} = \text{tr}(\mathbf{J}(\mathbf{p})^{-1}). \quad (21)$$

Combining (14b), (19), and (21), the SPEB can be expressed as (22) at the top of the next page. It is observed from (22) that the SPEB is a function of the HBF matrix $\mathbf{F}_{\text{RF}} \mathbf{F}_{\text{BB}}$. Therefore, we can improve the target localization accuracy by optimizing the HBF design.

B. Problem Formulation

Based on the above SPEB analysis, we formulate two HBF optimization problems in this subsection.

For the sensing-centric design, the digital beamformer and partially-connected analog beamformer are jointly optimized to minimize the sensing SPEB, while satisfying the communication SINR requirements, transmit power constraint, and unit modulus constraints. The sensing-centric HBF design problem can be formulated as

$$\min_{\mathbf{F}_{\text{RF}}, \mathbf{F}_{\text{BB}}} \text{SPEB}(\mathbf{F}_{\text{RF}}, \mathbf{F}_{\text{BB}}) \quad (23a)$$

$$\text{s.t. } \text{SINR}_k(\mathbf{F}_{\text{RF}}, \mathbf{F}_{\text{BB}}) \geq \Gamma_k, \forall k, \quad (23b)$$

$$\|\mathbf{F}_{\text{RF}} \mathbf{F}_{\text{BB}}\|_F^2 \leq P, \quad (23c)$$

$$\mathbf{F}_{\text{RF}} \in \mathcal{A}_p, \quad (23d)$$

where Γ_k represents the minimum QoS requirement for the k -th communication UE, P represents the transmit power budget, and \mathcal{A}_p represents the feasible set of analog beamformer

$$\text{SPEB}(\mathbf{F}_{\text{RF}}, \mathbf{F}_{\text{BB}}) = \text{tr} \left(\left(\sum_{m=1}^M \mathbf{v}_m \left(\frac{2T|\alpha_m|^2}{\sigma_n^2} \left(\text{tr}(\dot{\mathbf{A}}_m \mathbf{F}_{\text{RF}} \mathbf{F}_{\text{BB}} \mathbf{F}_{\text{BB}}^H \mathbf{F}_{\text{RF}}^H \dot{\mathbf{A}}_m^H) - \frac{|\text{tr}(\mathbf{A}_m \mathbf{F}_{\text{RF}} \mathbf{F}_{\text{BB}} \mathbf{F}_{\text{BB}}^H \mathbf{F}_{\text{RF}}^H \dot{\mathbf{A}}_m^H)|^2}{\text{tr}(\mathbf{A}_m \mathbf{F}_{\text{RF}} \mathbf{F}_{\text{BB}} \mathbf{F}_{\text{BB}}^H \mathbf{F}_{\text{RF}}^H \mathbf{A}_m^H)} \right) \right) \mathbf{v}_m^T \right)^{-1}. \quad (22)$$

in which each nonzero element of \mathbf{F}_{RF} should satisfy unit modulus constraint.

For the communication-centric design, the HBF optimization is formulated as the sum-rate maximization problem under the target localization accuracy constraint, which can be expressed as

$$\max_{\mathbf{F}_{\text{RF}}, \mathbf{F}_{\text{BB}}} \sum_{k=1}^K \log(1 + \text{SINR}_k(\mathbf{F}_{\text{RF}}, \mathbf{F}_{\text{BB}})) \quad (24a)$$

$$\text{s.t. } \text{SPEB}(\mathbf{F}_{\text{RF}}, \mathbf{F}_{\text{BB}}) \leq \epsilon_p, \quad (24b)$$

$$\|\mathbf{F}_{\text{RF}} \mathbf{F}_{\text{BB}}\|_F^2 \leq P, \quad (24c)$$

$$\mathbf{F}_{\text{RF}} \in \mathcal{A}_p, \quad (24d)$$

where ϵ_p represents the SPEB threshold of target localization. It is observed that both (23) and (24) are nonconvex problems due to the complicated SPEB expression, the highly coupled analog beamformer \mathbf{F}_{RF} and digital beamformer \mathbf{F}_{BB} , as well as nonconvex unit modulus constraints.

IV. SENSING-CENTRIC HBF DESIGN

This section proposes an SDR-based alternating optimization algorithm for addressing the communication SINR-constrained sensing SPEB minimization problem.

A. Problem Reformulation

To tackle the complicated SPEB expression (23a), we introduce the auxiliary positive semidefinite matrix $\mathbf{U} \in \mathbb{C}^{2 \times 2}$. The objective function (23a) can be equivalently transformed into a tractable form by exploiting the proposition as follows.

Proposition 1. *The SPEB minimization in (23a) is equivalent to tackling the following problem (25)*

$$\min_{\mathbf{F}_{\text{RF}}, \mathbf{F}_{\text{BB}}, \mathbf{U}} \text{tr}(\mathbf{U}^{-1}) \quad (25a)$$

$$\text{s.t. } \sum_{m=1}^M \mathbf{v}_m J_{\theta_m \theta_m}^e \mathbf{v}_m^T \succeq \mathbf{U}, \quad (25b)$$

$$\mathbf{U} \succeq \mathbf{0}. \quad (25c)$$

Proof. See Appendix. \square

Based on **Proposition 1**, problem (23) can be equivalently reformulated as

$$\min_{\mathbf{F}_{\text{RF}}, \mathbf{F}_{\text{BB}}, \mathbf{U}} \text{tr}(\mathbf{U}^{-1}) \quad (26a)$$

$$\text{s.t. } (23b), (23c), (23d), (25b), (25c). \quad (26b)$$

By introducing the auxiliary variables $t_m, m = 1, \dots, M$, constraint (25b) can be equivalently transformed into the following two inequality constraints:

$$\sum_{m=1}^M \mathbf{v}_m \left(\frac{2T|\alpha_m|^2}{\sigma_n^2} t_m \right) \mathbf{v}_m^T \succeq \mathbf{U}, \quad (27a)$$

$$\text{tr}(\dot{\mathbf{A}}_m \mathbf{R}_X \dot{\mathbf{A}}_m^H) - \frac{|\text{tr}(\mathbf{A}_m \mathbf{R}_X \dot{\mathbf{A}}_m^H)|^2}{\text{tr}(\mathbf{A}_m \mathbf{R}_X \dot{\mathbf{A}}_m^H)} \geq t_m, \forall m. \quad (27b)$$

By using the Schur complement condition [32], constraint (27b) can be rewritten as

$$\begin{bmatrix} \text{tr}(\dot{\mathbf{A}}_m \mathbf{R}_X \dot{\mathbf{A}}_m^H) - t_m & \text{tr}(\mathbf{A}_m \mathbf{R}_X \dot{\mathbf{A}}_m^H) \\ \text{tr}(\dot{\mathbf{A}}_m \mathbf{R}_X \mathbf{A}_m^H) & \text{tr}(\mathbf{A}_m \mathbf{R}_X \mathbf{A}_m^H) \end{bmatrix} \succeq \mathbf{0}, \forall m. \quad (28)$$

Therefore, problem (26) can be equivalently reformulated as

$$\min_{\mathbf{F}_{\text{RF}}, \mathbf{F}_{\text{BB}}, \mathbf{U}, t_m} \text{tr}(\mathbf{U}^{-1}) \quad (29a)$$

$$\text{s.t. } (23b), (23c), (23d), (25c), (27a), (28). \quad (29b)$$

Subsequently, we design the digital beamformer and analog beamformer, respectively.

B. Digital Beamformer Design

In this subsection, the digital beamformer \mathbf{F}_{BB} is optimized with given the analog beamformer \mathbf{F}_{RF} . Exploiting the block diagonal structure of \mathbf{F}_{RF} , the transmit power can be rewritten as

$$\|\mathbf{F}_{\text{RF}} \mathbf{F}_{\text{BB}}\|_F^2 = \text{tr}(\mathbf{F}_{\text{RF}}^H \mathbf{F}_{\text{RF}} \mathbf{F}_{\text{BB}} \mathbf{F}_{\text{BB}}^H) = \frac{N_t}{N_{\text{RF}}} \text{tr}(\mathbf{F}_{\text{BB}} \mathbf{F}_{\text{BB}}^H). \quad (30)$$

The SINR constraint in (23b) can be rewritten as

$$(1 + \frac{1}{\Gamma_k}) \mathbf{f}_{\text{BB},k}^H \mathbf{F}_{\text{RF}}^H \mathbf{h}_k \mathbf{h}_k^H \mathbf{F}_{\text{RF}} \mathbf{f}_{\text{BB},k} \geq \sum_{j=1}^K \mathbf{f}_{\text{BB},j}^H \mathbf{F}_{\text{RF}}^H \mathbf{h}_k \mathbf{h}_k^H \mathbf{F}_{\text{RF}} \mathbf{f}_{\text{BB},j} + \sigma_n^2, \forall k. \quad (31)$$

Thus, the subproblem w.r.t. the digital beamformer \mathbf{F}_{BB} can be recast as

$$\min_{\mathbf{F}_{\text{BB}}, \mathbf{U}, t_m} \text{tr}(\mathbf{U}^{-1}) \quad (32a)$$

$$\text{s.t. } \begin{bmatrix} \text{tr}(\ddot{\Psi}_m \mathbf{F}_{\text{BB}} \mathbf{F}_{\text{BB}}^H) - t_m & \text{tr}(\dot{\Psi}_m \mathbf{F}_{\text{BB}} \mathbf{F}_{\text{BB}}^H) \\ \text{tr}(\dot{\Psi}_m^H \mathbf{F}_{\text{BB}} \mathbf{F}_{\text{BB}}^H) & \text{tr}(\Psi_m \mathbf{F}_{\text{BB}} \mathbf{F}_{\text{BB}}^H) \end{bmatrix} \succeq \mathbf{0}, \forall m, \quad (32b)$$

$$(1 + \frac{1}{\Gamma_k}) \mathbf{f}_{\text{BB},k}^H \tilde{\mathbf{H}}_k \mathbf{f}_{\text{BB},k} \geq \sum_{j=1}^K \mathbf{f}_{\text{BB},j}^H \tilde{\mathbf{H}}_k \mathbf{f}_{\text{BB},j} + \sigma_n^2, \forall k, \quad (32c)$$

$$\frac{N_t}{N_{\text{RF}}} \text{tr}(\mathbf{F}_{\text{BB}} \mathbf{F}_{\text{BB}}^H) \leq P, \quad (32d)$$

$$(25c), (27a), \quad (32e)$$

where we define

$$\ddot{\Psi}_m \triangleq \mathbf{F}_{\text{RF}}^H \dot{\mathbf{A}}_m^H \dot{\mathbf{A}}_m \mathbf{F}_{\text{RF}}, \quad (33a)$$

$$\dot{\Psi}_m \triangleq \mathbf{F}_{\text{RF}}^H \dot{\mathbf{A}}_m^H \mathbf{A}_m \mathbf{F}_{\text{RF}}, \quad (33b)$$

$$\Psi_m \triangleq \mathbf{F}_{\text{RF}}^H \mathbf{A}_m^H \mathbf{A}_m \mathbf{F}_{\text{RF}}, \quad (33c)$$

$$\tilde{\mathbf{H}}_k \triangleq \mathbf{F}_{\text{RF}}^H \mathbf{h}_k \mathbf{h}_k^H \mathbf{F}_{\text{RF}}. \quad (33d)$$

Problem (32) is nonconvex owing to the nonconvex quadratic constraint (32b) and constraint (32c). Therefore, we tackle the nonconvex problem (32) by adopting the SDR technique [33]. We define the auxiliary variables $\mathbf{W}_k = \mathbf{f}_{\text{BB},k} \mathbf{f}_{\text{BB},k}^H, \forall k$ that satisfy $\mathbf{W}_k \succeq \mathbf{0}$ and $\text{rank}(\mathbf{W}_k) = 1, \forall k$. However, the rank-one constraints $\text{rank}(\mathbf{W}_k) = 1, \forall k$ are nonconvex. To this end, we drop them and obtain the SDR problem of (32) as

$$\min_{\mathbf{W}_k, t_m} \text{tr}(\mathbf{U}^{-1}) \quad (34a)$$

$$\text{s.t.} \begin{bmatrix} \text{tr}(\ddot{\Psi}_m \sum_{k=1}^K \mathbf{W}_k) - t_m & \text{tr}(\dot{\Psi}_m \sum_{k=1}^K \mathbf{W}_k) \\ \text{tr}(\dot{\Psi}_m^H \sum_{k=1}^K \mathbf{W}_k) & \text{tr}(\Psi_m \sum_{k=1}^K \mathbf{W}_k) \end{bmatrix} \succeq \mathbf{0}, \forall m, \quad (34b)$$

$$(1 + \frac{1}{\Gamma_k}) \text{tr}(\tilde{\mathbf{H}}_k \mathbf{W}_k) \geq \sum_{j=1}^K \text{tr}(\tilde{\mathbf{H}}_k \mathbf{W}_j) + \sigma_n^2, \forall k, \quad (34c)$$

$$\text{tr}\left(\sum_{k=1}^K \mathbf{W}_k\right) \leq \frac{P N_{\text{RF}}}{N_t}, \quad (34d)$$

$$\mathbf{W}_k \succeq \mathbf{0}, \forall k, \quad (34e)$$

$$(25c), (27a). \quad (34f)$$

We can observe that problem (34) is a convex semidefinite programming (SDP) problem, which can be optimally solved by standard convex optimization solvers such as CVX. Let \mathbf{W}_k^* represent the optimal solution to problem (34). Nevertheless, the rank of \mathbf{W}_k^* may be larger than one due to the omission of the rank-one constraint. Therefore, we extract a feasible rank-one solution to the original problem (32) from \mathbf{W}_k^* via eigenvalue decomposition [33].

C. Analog Beamformer Design

With the digital beamformer \mathbf{F}_{BB} fixed, the analog beamformer \mathbf{F}_{RF} is optimized in this subsection. Leveraging the block diagonal structure, \mathbf{F}_{RF} can be rewritten as

$$\mathbf{F}_{\text{RF}} = \tilde{\mathbf{F}}_{\text{RF}} \Phi = \text{diag}(\mathbf{f}_{\text{RF}}) \Phi, \quad (35)$$

where $\tilde{\mathbf{F}}_{\text{RF}} = \text{blkdiag}\{\text{diag}(\mathbf{f}_1), \dots, \text{diag}(\mathbf{f}_{N_{\text{RF}}})\} \in \mathbb{C}^{N_t \times N_t}$ and $\mathbf{f}_{\text{RF}} = [\mathbf{f}_1^T, \dots, \mathbf{f}_{N_{\text{RF}}}^T]^T \in \mathbb{C}^{N_t \times 1}$ are respectively a diagonal matrix and a column vector composed of the nonzero elements of \mathbf{F}_{RF} , $\Phi = \text{blkdiag}\{\mathbf{1}, \mathbf{1}, \dots, \mathbf{1}\} \in \mathbb{C}^{N_t \times N_{\text{RF}}}$, and $\mathbf{1}$ is an N_t/N_{RF} dimensional vector with all elements being 1. Therefore, the covariance matrix in (10) can be rewritten as

$$\begin{aligned} \mathbf{R}_X &= \sum_{k=1}^K \text{diag}(\mathbf{f}_{\text{RF}}) \Phi \mathbf{f}_{\text{BB},k} \mathbf{f}_{\text{BB},k}^H \Phi^H \text{diag}(\mathbf{f}_{\text{RF}})^H \\ &= \sum_{k=1}^K \text{diag}(\Phi \mathbf{f}_{\text{BB},k}) \mathbf{f}_{\text{RF}} \mathbf{f}_{\text{RF}}^H \text{diag}(\Phi \mathbf{f}_{\text{BB},k})^H. \end{aligned} \quad (36)$$

For notational simplicity, we define

$$\ddot{\Pi}_m \triangleq \sum_{k=1}^K \text{diag}(\Phi \mathbf{f}_{\text{BB},k})^H \dot{\mathbf{A}}_m^H \dot{\mathbf{A}}_m \text{diag}(\Phi \mathbf{f}_{\text{BB},k}), \quad (37a)$$

$$\dot{\Pi}_m \triangleq \sum_{k=1}^K \text{diag}(\Phi \mathbf{f}_{\text{BB},k})^H \dot{\mathbf{A}}_m^H \mathbf{A}_m \text{diag}(\Phi \mathbf{f}_{\text{BB},k}), \quad (37b)$$

$$\Pi_m \triangleq \sum_{k=1}^K \text{diag}(\Phi \mathbf{f}_{\text{BB},k})^H \mathbf{A}_m^H \mathbf{A}_m \text{diag}(\Phi \mathbf{f}_{\text{BB},k}), \quad (37c)$$

$$\bar{\mathbf{H}}_{k,j} \triangleq \text{diag}(\Phi \mathbf{f}_{\text{BB},j})^H \mathbf{h}_k \mathbf{h}_k^H \text{diag}(\Phi \mathbf{f}_{\text{BB},j}). \quad (37d)$$

Therefore, the subproblem w.r.t. \mathbf{f}_{RF} can be represented as

$$\min_{\mathbf{f}_{\text{RF}}, \mathbf{U}, t_m} \text{tr}(\mathbf{U}^{-1}) \quad (38a)$$

$$\text{s.t.} \begin{bmatrix} \text{tr}(\ddot{\Pi}_m \mathbf{f}_{\text{RF}} \mathbf{f}_{\text{RF}}^H) - t_m & \text{tr}(\dot{\Pi}_m \mathbf{f}_{\text{RF}} \mathbf{f}_{\text{RF}}^H) \\ \text{tr}(\dot{\Pi}_m^H \mathbf{f}_{\text{RF}} \mathbf{f}_{\text{RF}}^H) & \text{tr}(\Pi_m \mathbf{f}_{\text{RF}} \mathbf{f}_{\text{RF}}^H) \end{bmatrix} \succeq \mathbf{0}, \forall m, \quad (38b)$$

$$(1 + \frac{1}{\Gamma_k}) \mathbf{f}_{\text{RF}}^H \bar{\mathbf{H}}_{k,k} \mathbf{f}_{\text{RF}} \geq \sum_{j=1}^K \mathbf{f}_{\text{RF}}^H \bar{\mathbf{H}}_{k,j} \mathbf{f}_{\text{RF}} + \sigma_n^2, \forall k, \quad (38c)$$

$$|[\mathbf{f}_{\text{RF}}]_i| = 1, \forall i, \quad (38d)$$

$$(25c), (27a). \quad (38e)$$

Problem (38) is still difficult to tackle since the quadratic constraints (38b) and (38c), as well as unit modulus constraints (38d) are nonconvex. The SDR method [33] is exploited to address problem (38). Specifically, we define the auxiliary variable $\mathbf{Q} = \mathbf{f}_{\text{RF}} \mathbf{f}_{\text{RF}}^H$ such that $\mathbf{Q} \succeq \mathbf{0}$ and $\text{rank}(\mathbf{Q}) = 1$. The rank-one constraint is omitted due to its nonconvexity. Thus, problem (38) can be relaxed as

$$\min_{\mathbf{Q}, \mathbf{U}, t_m} \text{tr}(\mathbf{U}^{-1}) \quad (39a)$$

$$\text{s.t.} \begin{bmatrix} \text{tr}(\ddot{\Pi}_m \mathbf{Q}) - t_m & \text{tr}(\dot{\Pi}_m \mathbf{Q}) \\ \text{tr}(\dot{\Pi}_m^H \mathbf{Q}) & \text{tr}(\Pi_m \mathbf{Q}) \end{bmatrix} \succeq \mathbf{0}, \forall m, \quad (39b)$$

$$(1 + \frac{1}{\Gamma_k}) \text{tr}(\bar{\mathbf{H}}_{k,k} \mathbf{Q}) \geq \sum_{j=1}^K \text{tr}(\bar{\mathbf{H}}_{k,j} \mathbf{Q}) + \sigma_n^2, \forall k, \quad (39c)$$

$$|[\mathbf{Q}]_{i,i}| = 1, \forall i, \quad (39d)$$

$$\mathbf{Q} \succeq \mathbf{0}, \quad (39e)$$

$$(25c), (27a). \quad (39f)$$

We observe that the relaxed problem (39) is a convex SDP problem. Let \mathbf{Q}^* represent the optimal solution to problem (39), which can be efficiently obtained by CVX toolbox. However, \mathbf{Q}^* may have high rank due to the omission of the rank-one constraint. Therefore, we construct a feasible rank-one solution by utilizing Gaussian randomization [33]. The detailed procedure is summarized in **Algorithm 1**.

D. Overall Algorithm

Based on the above design, the digital beamformer and analog beamformer are alternately updated until convergence. The proposed alternating optimization based on SDR (AO-SDR)

Algorithm 1 Gaussian randomization for obtaining the approximate optimal solution of analog beamformer

- 1: **Input:** Given the SDR solution \mathbf{Q}^* , and the number of Gaussian random samples N_{GR} .
- 2: Perform eigenvalue decomposition $\mathbf{Q}^* = \mathbf{V}_{\mathbf{Q}^*} \Sigma_{\mathbf{Q}^*} \mathbf{V}_{\mathbf{Q}^*}^H$;
- 3: Generate N_{GR} complex Gaussian random vectors $\mathbf{r}_l \sim \mathcal{CN}(\mathbf{0}, \mathbf{I}_{N_t})$, $l = 1, \dots, N_{\text{GR}}$;
- 4: Generate N_{GR} candidate solutions $\tilde{\mathbf{f}}_l = \exp(j \arg(\mathbf{V}_{\mathbf{Q}^*} \Sigma_{\mathbf{Q}^*}^{1/2} \mathbf{r}_l))$, $l = 1, \dots, N_{\text{GR}}$;
- 5: Select the solution that minimizes the sensing SPEB in (23a) while satisfying the communication SINR constraint in (23b) from all the candidate solutions as the approximate optimal solution of problem (23), i.e.,

$$l^* = \arg \min_{l=1, \dots, N_{\text{GR}}} \text{SPEB}(\tilde{\mathbf{f}}_l);$$
- 6: **Output:** Approximate optimal solution of analog beamformer $\mathbf{f}_{\text{RF}}^* = \tilde{\mathbf{f}}_{l^*}$.

algorithm for solving the communication SINR-constrained sensing SPEB minimization problem (23) is summarized in **Algorithm 2**.

Convergence Analysis: In each iteration of **Algorithm 2**, the optimal solutions of SDP problems (34) and (39) can be obtained by CVX. However, constructing the rank-one solution via eigenvalue decomposition or Gaussian randomization inevitably leads to slight performance loss. Therefore, during the alternating optimization procedure, the monotonicity of the objective value of problem (23) cannot be guaranteed theoretically [34]. Nevertheless, the proposed AO-SDR algorithm typically can converge to a stationary point in practice.

Complexity Analysis: The complexity of **Algorithm 2** mainly comes from problem (34) and problem (39), which are solved by utilizing the interior point method [35]. Given a solution accuracy ϵ , the computational complexities for solving problem (34) and problem (39) are given by $\mathcal{O}(\log(1/\epsilon) K^{6.5} N_{\text{RF}}^{6.5})$ and $\mathcal{O}(\log(1/\epsilon) N_t^{6.5})$, respectively. Moreover, the complexity of the rank-one solution construction via eigenvalue decomposition and Gaussian randomization is also considered. For the digital beamformer design, the complexity for constructing rank-one solutions by performing eigenvalue decomposition on \mathbf{W}_k^* , $\forall k$ is given by $\mathcal{O}(K N_{\text{RF}}^3)$. For the analog beamformer design, the complexity for constructing rank-one solution via Gaussian randomization in **Algorithm 1** is analyzed as follows. Specifically, in step 2, the complexity for performing eigenvalue decomposition on \mathbf{Q}^* is given by $\mathcal{O}(N_t^3)$. In step 4, the complexity for generating N_{GR} candidate solutions is given by $\mathcal{O}(N_{\text{GR}} N_t^2)$. In step 5, the complexities for calculating the communication SINR in (23b) and calculating the sensing SPEB in (23a) are given by $\mathcal{O}(N_{\text{GR}} K^2 N_t N_{\text{RF}})$ and $\mathcal{O}(N_{\text{GR}} M K N_t^2)$, respectively.

Algorithm 2 Proposed AO-SDR algorithm for solving SINR-constrained SPEB minimization problem (23)

- 1: **Input:** Initialize the analog beamformer $\mathbf{F}_{\text{RF}}^{(0)}$, iteration index $n = 1$, and convergence threshold δ .
- 2: **repeat**
- 3: Update $\mathbf{F}_{\text{BB}}^{(n)}$ by solving problem (34);
- 4: Update $\mathbf{F}_{\text{RF}}^{(n)}$ by solving problem (39);
- 5: $n = n + 1$;
- 6: **until** The objective value of problem (23) converges.
- 7: **Output:** \mathbf{F}_{RF} , \mathbf{F}_{BB} .

Therefore, the total complexity of **Algorithm 2** is given by

$$\begin{aligned} \mathcal{O}\left(N_{\text{iter}} \left(\log(1/\epsilon) (N_t^{6.5} + K^{6.5} N_{\text{RF}}^{6.5}) \right. \right. \\ \left. \left. + N_{\text{GR}} (N_t^2 + K^2 N_t N_{\text{RF}} + M K N_t^2) + N_t^3 + K N_{\text{RF}}^3 \right) \right), \end{aligned} \quad (40)$$

where N_{iter} represents the number of iterations.

V. COMMUNICATION-CENTRIC HBF DESIGN

In this section, an alternating optimization algorithm based on FP technique is proposed for tackling the sensing SPEB-constrained sum-rate maximization problem.

A. Problem Reformulation

The sum-rate maximization problem (24) is difficult to tackle due to its complicated objective function (24a) with sum-of-logarithm-of-ratio form. To facilitate the optimization, we reformulate problem (24) by exploiting the FP method. Specifically, the objective function (24a) is first transformed into a sum-of-ratio form by utilizing the Lagrangian dual transform [36]. Towards this end, we introduce the auxiliary variable $\boldsymbol{\gamma} = [\gamma_1, \dots, \gamma_K]^T \in \mathbb{R}_+^{K \times 1}$ and recast (24a) as

$$\sum_{k=1}^K \log(1 + \gamma_k) - \sum_{k=1}^K \gamma_k + \sum_{k=1}^K \frac{(1 + \gamma_k) |\mathbf{h}_k^H \mathbf{F}_{\text{RF}} \mathbf{f}_{\text{BB},k}|^2}{\sum_{j=1}^K |\mathbf{h}_k^H \mathbf{F}_{\text{RF}} \mathbf{f}_{\text{BB},j}|^2 + \sigma_n^2}. \quad (41)$$

Then, the quadratic transform [36] is applied to tackle the sum-of-ratio term of (41). By defining the auxiliary variable $\boldsymbol{\beta} = [\beta_1, \dots, \beta_K]^T \in \mathbb{C}^{K \times 1}$, problem (24) can be equivalently reformulated as

$$\max_{\mathbf{F}_{\text{RF}}, \mathbf{F}_{\text{BB}}, \boldsymbol{\gamma}, \boldsymbol{\beta}} f(\mathbf{F}_{\text{RF}}, \mathbf{F}_{\text{BB}}, \boldsymbol{\gamma}, \boldsymbol{\beta}) \quad (42a)$$

$$\text{s.t. } (24b), (24c), (24d), \quad (42b)$$

where the objective function $f(\mathbf{F}_{\text{RF}}, \mathbf{F}_{\text{BB}}, \boldsymbol{\gamma}, \boldsymbol{\beta})$ can be represented as (43) at the bottom of the next page.

In the following, we alternately optimize the analog beamformer \mathbf{F}_{RF} , digital beamformer \mathbf{F}_{BB} , and auxiliary variables $\boldsymbol{\gamma}$ and $\boldsymbol{\beta}$ until the objective value converges. The detailed solutions are presented as follows.

Update $\boldsymbol{\gamma}$: With the analog beamformer \mathbf{F}_{RF} , digital beamformer \mathbf{F}_{BB} , and auxiliary variable $\boldsymbol{\beta}$ fixed, the subproblem w.r.t. the auxiliary variable γ_k is an unconstrained convex

problem. According to the first-order optimality condition, the optimal solution of γ_k can be given by

$$\gamma_k^* = \frac{|\mathbf{h}_k^H \mathbf{F}_{\text{RF}} \mathbf{f}_{\text{BB},k}|^2}{\sum_{j=1, j \neq k}^K |\mathbf{h}_k^H \mathbf{F}_{\text{RF}} \mathbf{f}_{\text{BB},j}|^2 + \sigma_n^2}, \forall k. \quad (44)$$

Update β : Similarly, the optimal solution of β_k can be calculated by solving $\partial f(\mathbf{F}_{\text{RF}}, \mathbf{F}_{\text{BB}}, \boldsymbol{\gamma}, \boldsymbol{\beta}) / \partial \beta_k = 0$ as

$$\beta_k^* = \frac{\sqrt{(1 + \rho_k)} \mathbf{h}_k^H \mathbf{F}_{\text{RF}} \mathbf{f}_{\text{BB},k}}{\sum_{j=1}^K |\mathbf{h}_k^H \mathbf{F}_{\text{RF}} \mathbf{f}_{\text{BB},j}|^2 + \sigma_n^2}, \forall k. \quad (45)$$

B. Digital Beamformer Design

Update \mathbf{F}_{BB} : With the analog beamformer \mathbf{F}_{RF} and the auxiliary variables $\boldsymbol{\gamma}$ and $\boldsymbol{\beta}$ fixed, we optimize the digital beamformer \mathbf{F}_{BB} . To simplify the notation of constraint (24b), we introduce the auxiliary positive semidefinite matrix $\mathbf{U} \in \mathbb{C}^{2 \times 2}$ and the auxiliary variables $t_m, m = 1, \dots, M$. Exploiting the matrix monotonicity and the block diagonal structure of \mathbf{F}_{RF} as shown in Section IV-B, the subproblem w.r.t. the digital beamformer \mathbf{F}_{BB} can be equivalently reformulated as

$$\min_{\substack{\mathbf{F}_{\text{BB}}, \\ \mathbf{U}, t_m}} \sum_{k=1}^K \mathbf{f}_{\text{BB},k}^H \mathbf{A} \mathbf{f}_{\text{BB},k} - \sum_{k=1}^K 2 \operatorname{Re} \{ \mathbf{f}_{\text{BB},k}^H \mathbf{b}_k \} \quad (46a)$$

$$\text{s.t. } \operatorname{tr} (\mathbf{U}^{-1}) \leq \epsilon_p, \quad (46b)$$

$$\mathbf{U} \succeq \mathbf{0}, \quad (46c)$$

$$\sum_{m=1}^M \mathbf{v}_m \left(\frac{2T|\alpha_m|^2}{\sigma_n^2} t_m \right) \mathbf{v}_m^T \succeq \mathbf{U}, \quad (46d)$$

$$\begin{bmatrix} \operatorname{tr}(\ddot{\Psi}_m \mathbf{F}_{\text{BB}} \mathbf{F}_{\text{BB}}^H) - t_m & \operatorname{tr}(\dot{\Psi}_m \mathbf{F}_{\text{BB}} \mathbf{F}_{\text{BB}}^H) \\ \operatorname{tr}(\dot{\Psi}_m^H \mathbf{F}_{\text{BB}} \mathbf{F}_{\text{BB}}^H) & \operatorname{tr}(\Psi_m \mathbf{F}_{\text{BB}} \mathbf{F}_{\text{BB}}^H) \end{bmatrix} \succeq \mathbf{0}, \forall m, \quad (46e)$$

$$\frac{N_t}{N_{\text{RF}}} \operatorname{tr}(\mathbf{F}_{\text{BB}} \mathbf{F}_{\text{BB}}^H) \leq P, \quad (46f)$$

where we define

$$\mathbf{A} \triangleq \sum_{k=1}^K |\beta_k|^2 \mathbf{F}_{\text{RF}}^H \mathbf{h}_k \mathbf{h}_k^H \mathbf{F}_{\text{RF}}, \quad (47a)$$

$$\mathbf{b}_k \triangleq \sqrt{(1 + \gamma_k)} \beta_k \mathbf{F}_{\text{RF}}^H \mathbf{h}_k. \quad (47b)$$

Problem (46) is a nonconvex quadratically constrained quadratic programming (QCQP) problem due to the quadratic objective function (46a) and the nonconvex quadratic constraint (46e). To handle problem (46), we define the auxiliary variables $\mathbf{W}_k = \mathbf{f}_{\text{BB},k} \mathbf{f}_{\text{BB},k}^H, \forall k$ such that $\mathbf{W}_k \succeq \mathbf{0}$ and $\operatorname{rank}(\mathbf{W}_k) = 1, \forall k$. To facilitate the optimization, we drop

the nonconvex rank-one constraints and reformulate the SDR problem of problem (46) as

$$\min_{\substack{\mathbf{w}_k, \mathbf{f}_{\text{BB},k}, \\ \mathbf{U}, t_m}} \operatorname{tr} \left(\mathbf{A} \sum_{k=1}^K \mathbf{W}_k \right) - \sum_{k=1}^K 2 \operatorname{Re} \{ \mathbf{f}_{\text{BB},k}^H \mathbf{b}_k \} \quad (48a)$$

$$\text{s.t. } \begin{bmatrix} \operatorname{tr}(\ddot{\Psi}_m \sum_{k=1}^K \mathbf{W}_k) - t_m & \operatorname{tr}(\dot{\Psi}_m \sum_{k=1}^K \mathbf{W}_k) \\ \operatorname{tr}(\dot{\Psi}_m^H \sum_{k=1}^K \mathbf{W}_k) & \operatorname{tr}(\Psi_m \sum_{k=1}^K \mathbf{W}_k) \end{bmatrix} \succeq \mathbf{0}, \forall m, \quad (48b)$$

$$\operatorname{tr} \left(\sum_{k=1}^K \mathbf{W}_k \right) \leq \frac{P N_{\text{RF}}}{N_t}, \quad (48c)$$

$$\mathbf{W}_k = \mathbf{f}_{\text{BB},k} \mathbf{f}_{\text{BB},k}^H, \forall k, \quad (48d)$$

$$\mathbf{W}_k \succeq \mathbf{0}, \forall k, \quad (48e)$$

$$(46b), (46c), (46d). \quad (48f)$$

Note that problem (48) is still nonconvex since the equality constraint (48d) is nonconvex. According to [37], the equality constraint $\mathbf{W}_k = \mathbf{f}_{\text{BB},k} \mathbf{f}_{\text{BB},k}^H, \forall k$ can be equivalently converted into the two inequality constraints as follows:

$$\begin{bmatrix} \mathbf{W}_k & \mathbf{f}_{\text{BB},k} \\ \mathbf{f}_{\text{BB},k}^H & 1 \end{bmatrix} \succeq \mathbf{0}, \forall k, \quad (49a)$$

$$\operatorname{tr}(\mathbf{W}_k) - \mathbf{f}_{\text{BB},k}^H \mathbf{f}_{\text{BB},k} \leq 0, \forall k. \quad (49b)$$

However, constraint (49b) is nonconvex. By dropping the constraint (49b), problem (48) can be further relaxed as

$$\min_{\substack{\mathbf{w}_k, \mathbf{f}_{\text{BB},k}, \\ \mathbf{U}, t_m}} \operatorname{tr} \left(\mathbf{A} \sum_{k=1}^K \mathbf{W}_k \right) - \sum_{k=1}^K 2 \operatorname{Re} \{ \mathbf{f}_{\text{BB},k}^H \mathbf{b}_k \} \quad (50a)$$

$$\text{s.t. } (46b), (46c), (46d), (46e), (48b), (48c), (48e), (49a). \quad (50b)$$

We observe that problem (50) is convex and its optimal solution can be efficiently obtained by CVX toolbox.

C. Analog Beamformer Design

Update \mathbf{F}_{RF} : With the digital beamformer \mathbf{F}_{BB} and the auxiliary variables $\boldsymbol{\gamma}$ and $\boldsymbol{\beta}$ fixed, we optimize the analog beamformer \mathbf{F}_{RF} . Leveraging the block diagonal structure of \mathbf{F}_{RF} as shown in Section IV-C, the subproblem w.r.t. \mathbf{F}_{RF} can be equivalently rewritten as the following subproblem w.r.t. \mathbf{f}_{RF} :

$$\min_{\mathbf{f}_{\text{RF}}, \mathbf{U}, t_m} \mathbf{f}_{\text{RF}}^H \mathbf{C} \mathbf{f}_{\text{RF}} - 2 \operatorname{Re} \{ \mathbf{f}_{\text{RF}}^H \mathbf{e} \} \quad (51a)$$

$$\text{s.t. } \operatorname{tr}(\mathbf{U}^{-1}) \leq \epsilon_p, \quad (51b)$$

$$\mathbf{U} \succeq \mathbf{0}, \quad (51c)$$

$$\sum_{m=1}^M \mathbf{v}_m \left(\frac{2T|\alpha_m|^2}{\sigma_n^2} t_m \right) \mathbf{v}_m^T \succeq \mathbf{U}, \quad (51d)$$

$$\begin{bmatrix} \operatorname{tr}(\ddot{\Pi}_m \mathbf{f}_{\text{RF}} \mathbf{f}_{\text{RF}}^H) - t_m & \operatorname{tr}(\dot{\Pi}_m \mathbf{f}_{\text{RF}} \mathbf{f}_{\text{RF}}^H) \\ \operatorname{tr}(\dot{\Pi}_m^H \mathbf{f}_{\text{RF}} \mathbf{f}_{\text{RF}}^H) & \operatorname{tr}(\Pi_m \mathbf{f}_{\text{RF}} \mathbf{f}_{\text{RF}}^H) \end{bmatrix} \succeq \mathbf{0}, \forall m, \quad (51e)$$

$$|\mathbf{f}_{\text{RF}}|_i = 1, \forall i, \quad (51f)$$

$$f(\mathbf{F}_{\text{RF}}, \mathbf{F}_{\text{BB}}, \boldsymbol{\gamma}, \boldsymbol{\beta}) = \sum_{k=1}^K \log(1 + \gamma_k) - \sum_{k=1}^K \gamma_k + \sum_{k=1}^K 2\sqrt{(1 + \gamma_k)} \operatorname{Re} \{ \beta_k^* \mathbf{h}_k^H \mathbf{F}_{\text{RF}} \mathbf{f}_{\text{BB},k} \} - \sum_{k=1}^K |\beta_k|^2 \left(\sum_{j=1}^K |\mathbf{h}_k^H \mathbf{F}_{\text{RF}} \mathbf{f}_{\text{BB},j}|^2 + \sigma_n^2 \right). \quad (43)$$

where we define

$$\mathbf{C} \triangleq \sum_{j=1}^K \text{diag}(\Phi \mathbf{f}_{\text{BB},j})^H \left(\sum_{k=1}^K |\beta_k|^2 \mathbf{h}_k \mathbf{h}_k^H \right) \text{diag}(\Phi \mathbf{f}_{\text{BB},j}), \quad (52a)$$

$$\mathbf{e} \triangleq \sum_{k=1}^K \sqrt{(1 + \gamma_k)} \beta_k \text{diag}(\Phi \mathbf{f}_{\text{BB},j})^H \mathbf{h}_k. \quad (52b)$$

Notice that since both the quadratic constraint (51e) and unit modulus constraint (51f) are nonconvex, problem (51) is a nonconvex QCQP problem. To deal with the above problem, we define the auxiliary variable $\mathbf{Q} = \mathbf{f}_{\text{RF}} \mathbf{f}_{\text{RF}}^H$ such that $\mathbf{Q} \succeq 0$ and $\text{rank}(\mathbf{Q}) = 1$. By omitting $\text{rank}(\mathbf{Q}) = 1$, we obtain a relaxed version of problem (51) as

$$\min_{\mathbf{Q}, \mathbf{f}_{\text{RF}}, \mathbf{U}, t_m} \text{tr}(\mathbf{CQ}) - 2\text{Re}\{\mathbf{f}_{\text{RF}}^H \mathbf{e}\} \quad (53a)$$

$$\text{s.t. } \begin{bmatrix} \text{tr}(\tilde{\mathbf{\Pi}}_m \mathbf{Q}) - t_m & \text{tr}(\dot{\mathbf{\Pi}}_m \mathbf{Q}) \\ \text{tr}(\tilde{\mathbf{\Pi}}_m^H \mathbf{Q}) & \text{tr}(\mathbf{\Pi}_m \mathbf{Q}) \end{bmatrix} \succeq 0, \forall m, \quad (53b)$$

$$|\mathbf{Q}|_{i,i} = 1, \forall i, \quad (53c)$$

$$\mathbf{Q} \succeq 0, \quad (53d)$$

$$\mathbf{Q} = \mathbf{f}_{\text{RF}} \mathbf{f}_{\text{RF}}^H, \quad (53e)$$

$$(51b), (51c), (51d). \quad (53f)$$

However, problem (53) is still nonconvex due to the nonconvex equality constraint (53e). Similar to Section V-B, we transform the equality constraint $\mathbf{Q} = \mathbf{f}_{\text{RF}} \mathbf{f}_{\text{RF}}^H$ into the following two inequality constraints:

$$\begin{bmatrix} \mathbf{Q} & \mathbf{f}_{\text{RF}} \\ \mathbf{f}_{\text{RF}}^H & 1 \end{bmatrix} \succeq 0, \quad (54a)$$

$$\text{tr}(\mathbf{Q}) - \mathbf{f}_{\text{RF}}^H \mathbf{f}_{\text{RF}} \leq 0. \quad (54b)$$

By dropping the nonconvex constraint (54b), problem (53) is relaxed as

$$\min_{\mathbf{Q}, \mathbf{f}_{\text{RF}}, \mathbf{U}, t_m} \text{tr}(\mathbf{CQ}) - 2\text{Re}\{\mathbf{f}_{\text{RF}}^H \mathbf{e}\} \quad (55a)$$

$$\text{s.t. } (51b), (51c), (51d), (53b), (53c), (53d), (54a). \quad (55b)$$

It is observed that the relaxed problem (55) is convex. We can obtain the optimal solution of this problem by CVX toolbox.

D. Overall Algorithm

Based on the aforementioned optimization, the auxiliary variables γ and β , digital beamformer \mathbf{F}_{BB} , and analog beamformer \mathbf{F}_{RF} are alternately updated until convergence. The proposed alternating optimization based on FP (AO-FP) algorithm for solving the sensing SPEB-constrained communication sum-rate maximization problem (24) is summarized in **Algorithm 3**.

Convergence Analysis: The optimal closed-form solutions of γ and β are obtained based on (44) and (45), respectively, and the locally optimal solutions of \mathbf{F}_{BB} and \mathbf{F}_{RF} are obtained through convex relaxation. Thus, the objective value of problem (24) is monotonically nondecreasing [38]. Since the transmit power is limited, the sum-rate in problem (24) has

Algorithm 3 Proposed AO-FP algorithm for solving SPEB-constrained sum-rate maximization problem (24)

-
- 1: **Input:** Initialize the analog beamformer $\mathbf{F}_{\text{RF}}^{(0)}$ and digital beamformer $\mathbf{F}_{\text{BB}}^{(0)}$, iteration index $n = 1$, and convergence threshold δ .
 - 2: **repeat**
 - 3: Update $\gamma^{(n)}$ by using equation (44);
 - 4: Update $\beta^{(n)}$ by using equation (45);
 - 5: Update $\mathbf{F}_{\text{BB}}^{(n)}$ by solving problem (50);
 - 6: Update $\mathbf{F}_{\text{RF}}^{(n)}$ by solving problem (55);
 - 7: $n = n + 1$;
 - 8: **until** The objective value of problem (24) converges.
 - 9: **Output:** \mathbf{F}_{RF} , \mathbf{F}_{BB} .
-

an upper bound. Therefore, **Algorithm 3** can be guaranteed to converge to a locally optimal solution of problem (24).

Complexity Analysis: The computational complexity of **Algorithm 3** mainly arises from the design of \mathbf{F}_{BB} and \mathbf{F}_{RF} , which are solved by utilizing the interior point method [35]. Given a solution accuracy ϵ , the computational complexities for solving problems (50) and (55) are given by $\mathcal{O}(\log(1/\epsilon) K^{6.5} N_{\text{RF}}^{6.5})$ and $\mathcal{O}(\log(1/\epsilon) N_t^{6.5})$, respectively. Therefore, the total complexity of **Algorithm 3** is given by $\mathcal{O}(N_{\text{iter}} \log(1/\epsilon) (N_t^{6.5} + K^{6.5} N_{\text{RF}}^{6.5}))$, where N_{iter} is the number of iterations.

VI. FDBF DESIGN

In this section, we briefly discuss the sensing-centric and communication-centric FDBF designs, which can provide performance upper bound for the corresponding HBF designs.

Let $\mathbf{F} = [\mathbf{f}_1, \dots, \mathbf{f}_K] \in \mathbb{C}^{N_t \times K}$ denote the FDBF matrix. Similar to the SPEB achieved by HBF in (22), the SPEB achieved by FDBF can be expressed as (56) at the top of the next page. For the FDBF design, the communication SINR of the k -th UE of can be represented as

$$\text{SINR}_k(\mathbf{F}) = \frac{|\mathbf{h}_k^H \mathbf{f}_k|^2}{\sum_{j=1, j \neq k}^K |\mathbf{h}_k^H \mathbf{f}_j|^2 + \sigma_n^2}. \quad (57)$$

Based on the above metrics, we formulate two FDBF design problems and present the corresponding solution strategies.

The sensing-centric FDBF design is formulated as the sensing SPEB minimization problem under the communication SINR constraints and transmit power constraint, which can be expressed as

$$\min_{\mathbf{F}} \text{SPEB}(\mathbf{F}) \quad (58a)$$

$$\text{s.t. } \text{SINR}_k(\mathbf{F}) \geq \Gamma_k, \forall k, \quad (58b)$$

$$\|\mathbf{F}\|_F^2 \leq P. \quad (58c)$$

Notice that problem (58) has a similar form to problem (23), except for the unit modulus constraints (23d). Therefore, problem (58) can be first reformulated as a tractable problem by utilizing the Schur complement as shown in Section IV-A. Then, the resulting problem can be efficiently solved by the SDR technique and eigenvalue decomposition as shown in Section IV-B.

$$\text{SPEB}(\mathbf{F}) = \text{tr} \left(\left(\sum_{m=1}^M \mathbf{v}_m \left(\frac{2T|\alpha_m|^2}{\sigma_n^2} \left(\text{tr}(\dot{\mathbf{A}}_m \mathbf{FF}^H \dot{\mathbf{A}}_m^H) - \frac{|\text{tr}(\mathbf{A}_m \mathbf{FF}^H \dot{\mathbf{A}}_m^H)|^2}{\text{tr}(\mathbf{A}_m \mathbf{FF}^H \mathbf{A}_m^H)} \right) \right) \mathbf{v}_m^T \right)^{-1} \right). \quad (56)$$

The communication-centric FDBF design is formulated to maximize the communication sum-rate subject to the target localization accuracy requirement and transmit power constraint, which can be given by

$$\max_{\mathbf{F}} \sum_{k=1}^K \log(1 + \text{SINR}_k(\mathbf{F})) \quad (59a)$$

$$\text{s.t. } \text{SPEB}(\mathbf{F}) \leq \epsilon_p, \quad (59b)$$

$$\|\mathbf{F}\|_F^2 \leq P. \quad (59c)$$

Similarly, problem (59) can be tackled by exploiting the FP-based problem reformulation in Section V-A and the convex relaxation-based digital beamformer design in Section V-B.

VII. SIMULATION RESULTS

In this section, simulation results are presented to verify the effectiveness of our proposed HBF algorithms. We consider a multi-static mmWave ISAC system consisting of one ISAC transmitter and $M = 3$ sensing receivers. Unless otherwise specified, the simulation parameters are set in Table II. The ISAC transmitter is located at (0m, 0m). The three sensing receivers are located at (100m, 0m), (0m, 100m), and (100m, 100m), respectively. The UEs are randomly distributed on an arc with the distance of 50m away from the ISAC transmitter and the angle ranging from 0 to $\pi/2$. The target is randomly distributed within a circular area with the center of (50m, 50m) and the radius of 20m. For a certain channel realization, the positions of the APs, UEs, and target are shown in Fig. 2.

For the target sensing, the target reflection coefficient is represented as

$$\alpha_m = \sqrt{\frac{G_T G_R \lambda^2 \sigma_{\text{rcs}}}{(4\pi)^3 d_T^2 d_{R,m}^2}}, \quad (60)$$

where G_T and G_R represent the antenna gains of the ISAC transmitter and sensing receivers, respectively, σ_{rcs} represents the RCS of the target, d_T represents the distance between the ISAC transmitter and the target, and $d_{R,m}$ represents the distance between the m -th sensing receiver and the target. We assume that the target reflection coefficient α_m is perfectly known in the subsequent numerical simulations.

For the multiuser communication, the mmWave channel between the ISAC transmitter and each UE includes one LOS path and three non-line-of-sight (NLOS) paths. The AODs of NLOS paths are randomly distributed in $[0, \pi/2]$. The channel gains satisfy Gaussian distribution $\mathcal{CN}(0, 10^{-0.1PL(d_k)})$. According to the empirical path loss model [39], the distance-dependent path loss is calculated by

$$PL(d_k) [\text{dB}] = a_1 + 10a_2 \log_{10}(d_k), \quad (61)$$

where d_k represents the distance between the ISAC transmitter and the k -th UE, a_1 represents the path loss at the reference distance of 1m, and a_2 represents the path loss exponent.

TABLE II
SIMULATION PARAMETERS

Parameter	Value
Number of APs $M + 1$	4
Number of ISAC transmitter	1
Number of sensing receivers M	3
Number of antennas of each AP $N_t(N_r)$	32
Number of RF chains of ISAC transmitter N_{RF}	4
Number of UEs K	3
Number of target	1
Number of snapshots T	30
Carrier frequency f_c	28 GHz
Noise power σ_n^2	-90 dBm
Transmit power P	30 dBm
Communication SINR threshold Γ_k	10 dB
Antenna gain $G_T(G_R)$	10 dBi
RCS of target σ_{rcs}	1 m ²
Convergence threshold δ	10 ⁻³

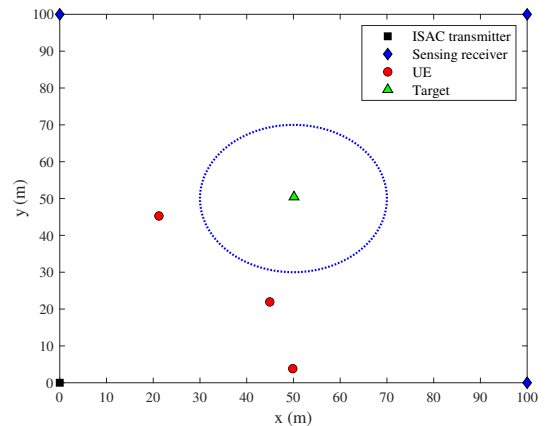


Fig. 2. The positions of the APs, UEs, and target.

According to [39], $a_1 = 61.4$, $a_2 = 2$ for the LOS path, and $a_1 = 72.0$, $a_2 = 2.92$ for the NLOS paths.

A. Communication SINR-Constrained SPEB Minimization

This subsection evaluates the effectiveness of our proposed AO-SDR algorithm for solving communication SINR-constrained sensing SPEB minimization problem (23). Unless otherwise specified, the SINR thresholds of communication UEs are set as $\Gamma_k = 10$ dB, $\forall k$. We compare the proposed **SPEB-Min based HBF** with the following three baseline schemes.

1) **SPEB-Min based FDBF:** The FDBF can be designed by utilizing our proposed SPEB minimization criterion and SDR technique. This scheme can provide a lower bound for the localization error achieved by our proposed HBF.

2) **Beampattern Approx. based HBF:** The beampattern of HBF is designed to approximate the ideal beampattern [10] by alternately optimizing the digital beamformer and analog beamformer.

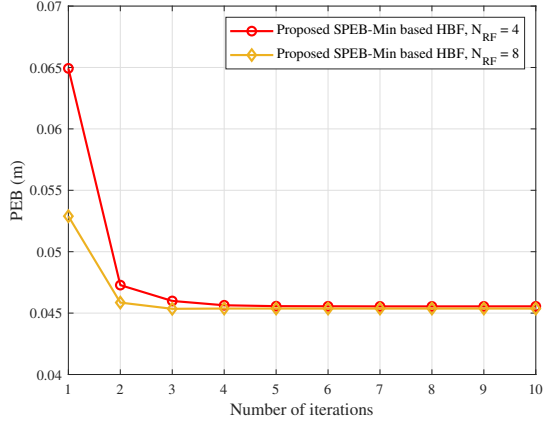


Fig. 3. Convergence of the proposed AO-SDR algorithm, where $N_t = N_r = 32$, $K = 3$, $\Gamma_k = 10$ dB, and $P = 30$ dBm.

3) **SIMO:** As depicted in footnote 1, in the first stage of target localization, the ISAC transmitter is equipped with single-antenna and cannot achieve directional beamforming.

For the above schemes, the MUSIC algorithm is applied in each sensing receiver to estimate the AOA of target echo, then all the estimated AOAs are transmitted to the central processor to cooperatively estimate the position of target by using least square method. The target localization error can be obtained by calculating the root mean square error (RMSE) between estimated position and real position. Note that the lower bound of RMSE for target localization can be given by the corresponding position error bound (PEB). The RMSE and PEB are respectively calculated as

$$\text{RMSE} = \sqrt{\frac{1}{N_{\text{mc}}} \sum_{n=1}^{N_{\text{mc}}} ((\hat{x}_n - x_n)^2 + (\hat{y}_n - y_n)^2)}, \quad (62\text{a})$$

$$\text{PEB} = \sqrt{\frac{1}{N_{\text{mc}}} \sum_{n=1}^{N_{\text{mc}}} \text{SPEB}_n}, \quad (62\text{b})$$

where N_{mc} represents the number of Monte Carlo trials, and $[x_n, y_n]$ and $[\hat{x}_n, \hat{y}_n]$ represent the real position and estimated position of the target in the n -th trial, respectively.

Fig. 3 evaluates the convergence behaviour of our proposed AO-SDR algorithm for SPEB minimization. As can be seen, the proposed AO-SDR algorithm rapidly converges within 10 iterations. In addition, as the number of RF chains increases, the convergence speed of the proposed AO-SDR algorithm is improved. This is because the increased number of RF chains provides more degrees of freedom for the design of analog beamformer and digital beamformer.

Fig. 4 shows the target localization accuracy versus transmit power. We observe that the proposed SPEB minimization based HBF achieves localization accuracy close to the FDBF counterpart and outperforms the beampattern approximation [10] based HBF, which demonstrates that exploiting the SPEB as the sensing performance metric of beamforming design can definitely enhance the target localization accuracy. Moreover, the proposed HBF and FDBF significantly outperform the SIMO case, which is because the proposed beamforming

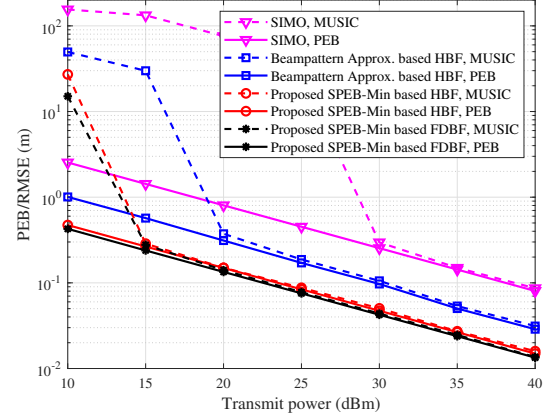


Fig. 4. Localization accuracy versus tranmsit power, where $N_t = N_r = 32$, $N_{\text{RF}} = 4$, $K = 3$, and $\Gamma_k = 10$ dB.

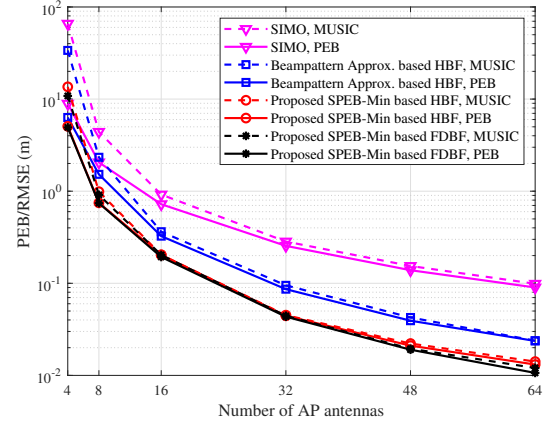


Fig. 5. Localization accuracy versus the number of AP antennas, where $N_t = N_r$, $N_{\text{RF}} = 4$, $K = 3$, $\Gamma_k = 10$ dB, and $P = 30$ dBm.

schemes can provide large array gain, thus improving the received SNR and enhancing the target localization accuracy. Specifically, the proposed HBF and FDBF can achieve the array gain of approximately 15dB compared to the SIMO scheme when the number of transmit antennas is 32. When the transmit power is 30dBm, the RMSEs of MUSIC-based localization for the SIMO, the beampattern approximation based HBF, the proposed SPEB minimization based HBF, and the proposed SPEB minimization based FDBF are approximately 30cm, 10cm, 5cm, and 4.5cm, respectively. Therefore, the proposed beamforming-enhanced localization approach can achieve centimeter level target localization accuracy. As expected, the PEB of the proposed SPEB minimization based beamforming design can provide a tight lower bound for the corresponding RMSE achieved by MUSIC-based localization, thereby verifying the validity of the proposed scheme.

Fig. 5 illustrates the target localization accuracy versus the number of AP antennas. We observe that the localization accuracy of the proposed SPEB minimization based HBF can approach that of FDBF and outperform the other baselines. Moreover, as the number of antennas increases, the localization accuracy is improved due to the increased array gain. When the number of antennas is sufficiently large, the PEBS

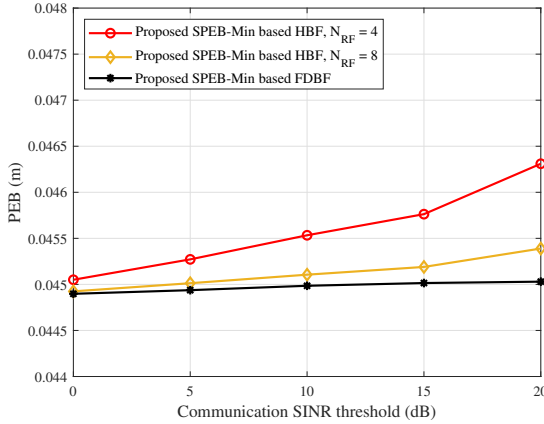


Fig. 6. Performance tradeoff between localization accuracy and communication SINR, where $N_t = N_r = 32$, $K = 3$, and $P = 30$ dBm.

of all the schemes can provide tight lower bounds for the corresponding RMSEs achieved by MUSIC-based localization.

Fig. 6 depicts the performance tradeoff between target localization accuracy and communication SINR requirement. It is seen that the target localization accuracy deteriorates as the SINR threshold Γ_k of communication UEs increases. This is due to the fact that the target localization and multiuser communication during ISAC stage share the same transmit power resource. When the communication QoS demand improves, more power is allocated to communication UEs, thus leading to the degradation of target localization performance. Furthermore, as the number of RF chains increases, the performance gap between the proposed HBF and FDBF gradually reduces.

B. Sensing SPEB-Constrained Sum-Rate Maximization

This subsection verifies the validity of our proposed AO-FP algorithm for solving SPEB-constrained sum-rate maximization problem (24). Unless otherwise specified, the SPEB threshold of target localization is set as $\epsilon_p = 0.09$ m², i.e., the PEB threshold is $\sqrt{\epsilon_p} = 0.3$ m. The proposed **Sum-Rate-Max based HBF** is compared with the following two baseline schemes.

1) **Sum-Rate-Max based FDBF:** Our proposed AO-FP algorithm can also be applied to this case by replacing HBF with FDBF. This scheme can provide a upper bound of sum-rate for our proposed HBF.

2) **Two-Stage based HBF:** In the first stage, the FDBF matrix is obtained by utilizing the same approach as **Sum-Rate-Max based FDBF**. In the second stage, the digital beamformer and analog beamformer are alternately updated to minimize the Euclidean distance between the HBF matrix and the FDBF matrix [15], which can be formulated as

$$\min_{\mathbf{F}_{RF}, \mathbf{F}_{BB}} \|\mathbf{F} - \mathbf{F}_{RF}\mathbf{F}_{BB}\|_F^2 \quad (63a)$$

$$\text{s.t. } \|\mathbf{F}_{RF}\mathbf{F}_{BB}\|_F^2 \leq P, \quad (63b)$$

$$\mathbf{F}_{RF} \in \mathcal{A}_p. \quad (63c)$$

Please refer to [15] for the detailed solution strategy. Notice that the above matrix approximation based approach is tailored

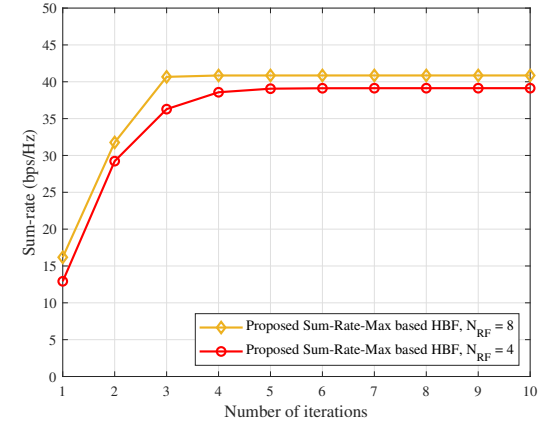


Fig. 7. Convergence of the proposed AO-FP algorithm, where $N_t = N_r = 32$, $K = 3$, $\epsilon_p = 0.09$ m², and $P = 30$ dBm.

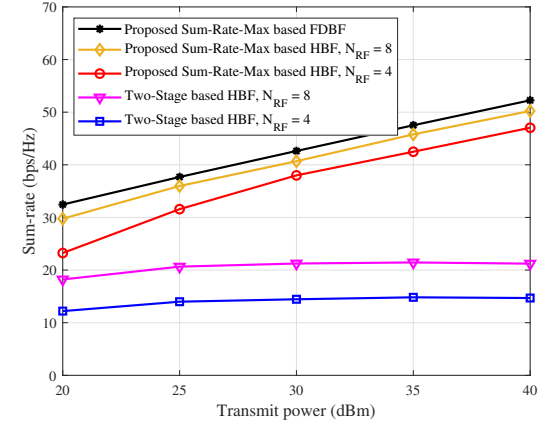


Fig. 8. Sum-rate versus transmit power, where $N_t = N_r = 32$, $K = 3$, and $\epsilon_p = 0.09$ m².

for single-user mmWave communication-only systems [14], [15]. It is not guaranteed that the solution obtained by tackling problem (63) always satisfies the sensing SPEB constraint (24b).

In Fig. 7, we present the convergence behaviour of our proposed AO-FP algorithm for sum-rate maximization. We observe that as the number of iterations increases, the sum-rate of our proposed AO-FP algorithm is monotonically increasing and quickly converges within several iterations. Moreover, when the number of RF chains increases, the sum-rate is improved and the convergence speed becomes faster.

Fig. 8 illustrates the sum-rate achieved by the proposed AO-FP algorithm versus transmit power. We observe that the proposed AO-FP based HBF design achieves sum-rate close to the FDBF counterpart, thereby significantly reducing hardware cost without obvious performance loss. Meanwhile, the proposed AO-FP based HBF design significantly outperforms the existing two-stage based HBF [15]. This is due to the fact that the matrix approximation based two-stage approach is designed for single-user communication-only systems [14], [15] and inevitably causes serious inter-user interference in our proposed multiuser ISAC system, thus leading to obvious sum-rate performance degradation.

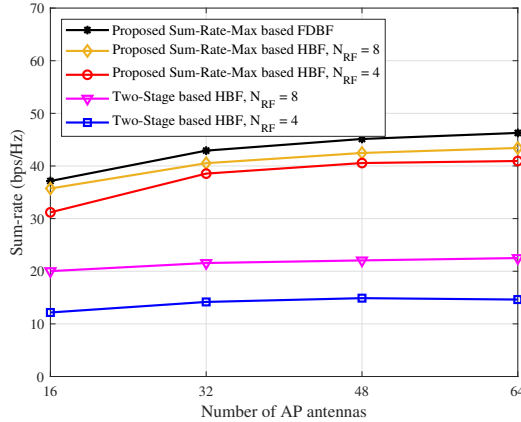


Fig. 9. Sum-rate versus the number of AP antennas, where $N_t = N_r$, $K = 3$, $\epsilon_p = 0.09 \text{ m}^2$, and $P = 30 \text{ dBm}$.

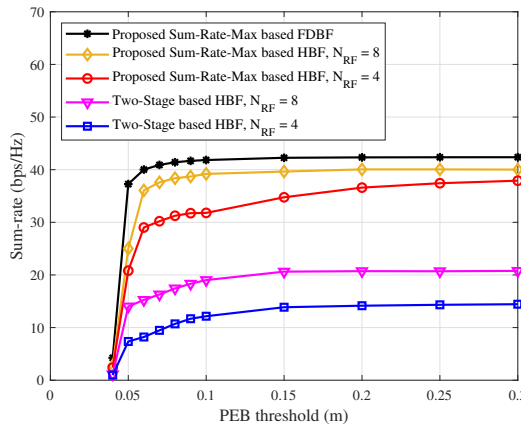


Fig. 10. Performance tradeoff between communication sum-rate and localization accuracy, where $N_t = N_r = 32$, $K = 3$, and $P = 30 \text{ dBm}$.

Fig. 9 depicts the impact of the number of AP antennas on the sum-rate performance. As the number of antennas increases, the proposed AO-FP based HBF design persistently approaches the FDBF and exhibits the increasing performance gain compared to the two-stage approach. Nevertheless, the performance improvement of the two-stage approach tends to stagnate due to the failed mitigation of multiuser interference. In contrast, the proposed HBF design can sufficiently exploit the large array gain provided by MIMO to improve sum-rate performance. In addition, as the number of RF chains increases, the sum-rate of the proposed AO-FP based HBF is improved. This is because the increased number of RF chains provides more degrees of freedom for multiuser interference mitigation.

Fig. 10 shows the performance tradeoff between communication sum-rate and target localization accuracy. It is seen that the sum-rate achieved by all the schemes deteriorates as the PEB threshold $\sqrt{\epsilon_p}$ decreases. In other words, the more stringent requirement of target localization accuracy leads to the more obvious degradation of communication sum-rate, which reveals the performance tradeoff between sensing and communication under limited resources. Furthermore, as the number of RF chains increases, the performance gap between

the proposed HBF and FDBF decreases, thus reflecting the tradeoff between performance and hardware cost.

VIII. CONCULTION

This paper investigated HBF design for mmWave MIMO ISAC systems with multi-static cooperative localization. The SPEB of AOA-based multi-static cooperative localization was derived to characterize the target localization accuracy. On this basis, two HBF design problems were investigated. For the sensing-centric design, we proposed an AO-SDR algorithm for addressing the communication SINR-constrained sensing SPEB minimization problem. For the communication-centric design, an AO-FP algorithm was proposed for solving the sensing SPEB-constrained communication sum-rate maximization problem. Simulation results showed that the proposed AO-SDR based sensing-centric HBF design can achieve localization accuracy close to the FDBF and outperform other baseline schemes, and the proposed AO-FP based communication-centric HBF design can achieve significant sum-rate performance improvement compared to the existing scheme.

For future work, some valuable research directions are discussed as follows.

- This paper considered two-dimensional target localization based on only azimuth AOAs. In fact, it is of great significance to acquire the three-dimensional position of target, especially for the emerging low-altitude economy scenario. By equipping all the APs with uniform planar arrays, our work can also be extended to achieve three-dimensional target localization based on both azimuth AOAs and elevation AOAs.
- This paper considered the multi-static single-target scenario. In the multi-static multi-target scenario, it is challenging to match the measurements (e.g., AOAs and TOAs) corresponding to the same target from different sensing receivers, thereby requiring an efficient data association algorithm [40]–[42].
- This paper investigated multi-static ISAC systems with cooperative passive sensing. Motivated by cell-free massive MIMO, how to design the cooperative beamforming in multi-static ISAC systems based on cooperative active and passive sensing for further improving communication capacity and sensing accuracy is an interesting problem.
- This paper assumed that the synchronization among APs and CSI are perfect. It is worth investigating the robust cooperative beamforming in multi-static ISAC systems under imperfect CSI and synchronization.

APPENDIX PROOF OF PROPOSITION 1

For a positive semidefinite matrix \mathbf{X} , the function $\text{tr}(\mathbf{X}^{-1})$ is monotonically decreasing on the positive semidefinite matrix space. From (19), we observe that the FIM of AOA-based multi-static cooperative localization $\sum_{m=1}^M \mathbf{v}_m J_{\theta_m \theta_m}^e \mathbf{v}_m^T$ is a positive semidefinite matrix. Leveraging the matrix monotonicity, minimizing $\text{tr}\left(\left(\sum_{m=1}^M \mathbf{v}_m J_{\theta_m \theta_m}^e \mathbf{v}_m^T\right)^{-1}\right)$ can be

equivalently transformed into minimizing $\text{tr}(\mathbf{U}^{-1})$ subject to the following two constraints:

$$\sum_{m=1}^M \mathbf{v}_m J_{\theta_m \theta_m}^e \mathbf{v}_m^T \succeq \mathbf{U}, \quad (64a)$$

$$\mathbf{U} \succeq \mathbf{0}. \quad (64b)$$

REFERENCES

- [1] F. Liu et al., "Integrated sensing and communications: Toward dual functional wireless networks for 6G and beyond," *IEEE J. Sel. Areas Commun.*, vol. 40, no. 6, pp. 1728–1767, Jun. 2022.
- [2] J. A. Zhang et al., "An overview of signal processing techniques for joint communication and radar sensing," *IEEE J. Sel. Topics Signal Process.*, vol. 15, no. 6, pp. 1295–1315, Nov. 2021.
- [3] J. A. Zhang, M. L. Rahman, K. Wu, X. Huang, Y. J. Guo, S. Chen, and J. Yuan, "Enabling joint communication and radar sensing in mobile networks-A survey," *IEEE Commun. Surveys Tuts.*, vol. 24, no. 1, pp. 306–345, 1st Quart., 2022.
- [4] A. Liu, et al., "A survey on fundamental limits of integrated sensing and communication," *IEEE Commun. Surveys Tuts.*, vol. 24, no. 2, pp. 994–1034, 2nd Quart. 2022.
- [5] N. González-Prelcic et al., "The integrated sensing and communication revolution for 6G: Vision, techniques, and applications," *Proc. IEEE*, vol. 112, no. 7, pp. 676–723, Jul. 2024.
- [6] Y. Xiong, F. Liu, Y. Cui, W. Yuan, T. X. Han, and G. Caire, "On the fundamental tradeoff of integrated sensing and communications under Gaussian channels," *IEEE Trans. Inf. Theory*, vol. 69, no. 9, pp. 5723–5751, Sep. 2023.
- [7] C. Sturm and W. Wiesbeck, "Waveform design and signal processing aspects for fusion of wireless communications and radar sensing," *Proc. IEEE*, vol. 99, no. 7, pp. 1236–1259, May 2011.
- [8] Z. Wei et al., "Integrated sensing and communication signals toward 5G-A and 6G: A survey," *IEEE Internet Things J.*, vol. 10, no. 13, pp. 11068–11092, 1 Jul., 2023.
- [9] F. Liu, C. Masouros, A. Petropulu, H. Griffiths, and L. Hanzo, "Joint radar and communication design: Applications, state-of-the-art, and the road ahead," *IEEE Trans. Commun.*, vol. 66, no. 6, pp. 3834–3862, Jun. 2020.
- [10] F. Liu, C. Masouros, A. Li, H. Sun, and L. Hanzo, "MU-MIMO communications with MIMO radar: From co-existence to joint transmission," *IEEE Trans. Wireless Commun.*, vol. 17, no. 4, pp. 2755–2770, Apr. 2018.
- [11] X. Liu, T. Huang, N. Shlezinger, Y. Liu, J. Zhou, and Y. C. Eldar, "Joint transmit beamforming for multiuser MIMO communications and MIMO radar," *IEEE Trans. Signal Process.*, vol. 68, pp. 3929–3944, Jun. 2020.
- [12] L. Chen, Z. Wang, Y. Du, Y. Chen, and F. R. Yu, "Generalized transceiver beamforming for DFRC with MIMO radar and MU-MIMO communication," *IEEE J. Sel. Areas Commun.*, vol. 40, no. 6, pp. 1795–1808, Jun. 2022.
- [13] F. Liu, Y.-F. Liu, A. Li, C. Masouros, and Y. C. Eldar, "Cramér-Rao bound optimization for joint radar-communication beamforming," *IEEE Trans. Signal Process.*, vol. 70, pp. 240–253, 2022.
- [14] O. El Ayach, S. Rajagopal, S. Abu-Surra, Z. Pi, and R. W. Heath, Jr., "Spatially sparse precoding in millimeter wave MIMO systems," *IEEE Trans. Wireless Commun.*, vol. 13, no. 3, pp. 1499–1513, Mar. 2014.
- [15] X. Yu, J.-C. Shen, J. Zhang, and K. B. Letaief, "Alternating minimization algorithms for hybrid precoding in millimeter wave MIMO systems," *IEEE J. Sel. Topics Signal Process.*, vol. 10, no. 3, pp. 485–500, May 2016.
- [16] M. Yuan, H. Wang, H. Yin, and D. He, "Alternating optimization based hybrid transceiver designs for wideband millimeter-wave massive multiuser MIMO-OFDM systems," *IEEE Trans. Wireless Commun.*, vol. 22, no. 12, pp. 9201–9217, Dec. 2023.
- [17] F. Liu and C. Masouros, "Hybrid beamforming with sub-arrayed MIMO radar: Enabling joint sensing and communication at mmWave band," in *Proc. IEEE Int. Conf. Acoust., Speech Signal Process. (ICASSP)*, May 2019, pp. 7770–7774.
- [18] Z. Cheng and B. Liao, "QoS-aware hybrid beamforming and DOA estimation in multi-carrier dual-function radar-communication systems," *IEEE J. Sel. Areas Commun.*, vol. 40, no. 6, pp. 1890–1905, Jun. 2022.
- [19] X. Wang, Z. Fei, J. A. Zhang, and J. Xu, "Partially-connected hybrid beamforming design for integrated sensing and communication systems," *IEEE Trans. Commun.*, vol. 70, no. 10, pp. 6648–6660, Oct. 2022.
- [20] J. A. Zhang, M. L. Rahman, X. Huang, Y. J. Guo, S. Chen, and R. W. Heath, "Perceptive mobile networks: Cellular networks with radio vision via joint communication and radar sensing," *IEEE Veh. Technol. Mag.*, vol. 16, no. 2, pp. 20–30, Jun. 2021.
- [21] Z. Wei et al., "Integrated sensing and communication enabled multiple base stations cooperative sensing towards 6G," *IEEE Netw.*, vol. 38, no. 4, pp. 207–215, Jul. 2024.
- [22] G. Cheng, Y. Fang, J. Xu, and D. W. K. Ng, "Optimal coordinated transmit beamforming for networked integrated sensing and communications," *IEEE Trans. Wireless Commun.*, vol. 23, no. 8, pp. 8200–8214, Aug. 2024.
- [23] X. Lou, W. Xia, K.-K. Wong, H. Zhao, T. Q. S. Quek, and H. Zhu, "Power optimization for integrated active and passive sensing in DFRC systems," *IEEE Trans. Wireless Commun.*, vol. 72, no. 6, pp. 3365–3377, Jun. 2024.
- [24] W. Mao, Y. Lu, C. -Y. Chi, B. Ai, Z. Zhong, and Z. Ding, "Communication-sensing region for cell-free massive MIMO ISAC systems," *IEEE Trans. Wireless Commun.*, vol. 23, no. 9, pp. 12396–12411, Sep. 2024.
- [25] Y. Huang, Y. Fang, X. Li, and J. Xu, "Coordinated power control for network integrated sensing and communication," *IEEE Trans. Veh. Technol.*, vol. 71, no. 12, pp. 13 361–13 365, Mar. 2022.
- [26] G. Liu et al., "Cooperative sensing for 6G mobile cellular networks: Feasibility, performance and field trial," *IEEE J. Sel. Areas Commun.*, vol. 42, no. 10, pp. 2863–2876, Oct. 2024.
- [27] R. Li, Z. Xiao, and Y. Zeng, "Towards seamless sensing coverage for cellular multi-static integrated sensing and communication," *IEEE Trans. Wireless Commun.*, vol. 23, no. 6, pp. 5363–5376, Jun. 2024.
- [28] T. Yang et al., "A unified tensor-based joint AUD and ISAC parameter estimation with large-scale user access," *IEEE Trans. Cognit. Commun. Netw.*, early access, 2025.
- [29] Y. Shen and M. Z. Win, "Fundamental limits of wideband localization—Part I: A general framework," *IEEE Trans. Inf. Theory*, vol. 56, no. 10, pp. 4956–4980, Oct. 2010.
- [30] Z. Abu-Shaban, X. Zhou, T. Abhayapala, G. Seco-Granados, and H. Wymeersch, "Error bounds for uplink and downlink 3D localization in 5G millimeter wave systems," *IEEE Trans. Wireless Commun.*, vol. 17, no. 8, pp. 4939–4954, Aug. 2018.
- [31] I. Bekerman and J. Tabrikian, "Target detection and localization using MIMO radars and sonars," *IEEE Trans. Signal Process.*, vol. 54, no. 10, pp. 3873–3883, Oct. 2006.
- [32] F. Zhang, *The Schur Complement and Its Applications*, vol. 4, Berlin, Germany: Springer-Verlag, 2005.
- [33] Z.-Q. Luo, W.-K. Ma, A. M.-C. So, Y. Ye, and S. Zhang, "Semidefinite relaxation of quadratic optimization problems," *IEEE Signal Process. Mag.*, vol. 27, no. 3, pp. 20–34, May 2010.
- [34] Z. Wang, X. Mu and Y. Liu, "STARS enabled integrated sensing and communications," *IEEE Trans. Wireless Commun.*, vol. 22, no. 10, pp. 6750–6765, Oct. 2023.
- [35] K.-C. Toh, "An inexact primal-dual path following algorithm for convex quadratic SDP," *Math. Programm.*, vol. 112, no. 1, pp. 221–254, 2008.
- [36] K. Shen and W. Yu, "Fractional programming for communication systems—Part I: Power control and beamforming," *IEEE Trans. Signal Process.*, vol. 66, no. 10, pp. 2616–2630, May 2018.
- [37] J. Zou et al., "Energy-efficient beamforming design for integrated sensing and communications systems," *IEEE Trans. Commun.*, vol. 72, no. 6, pp. 3766–3782, Jun. 2024.
- [38] M. Razaviyayn, M. Hong, and Z.-Q. Luo, "A unified convergence analysis of block successive minimization methods for nonsmooth optimization," *SIAM J. Optim.*, vol. 23, no. 2, pp. 1126–1153, 2013.
- [39] M. R. Akdeniz et al., "Millimeter wave channel modeling and cellular capacity evaluation," *IEEE J. Sel. Areas Commun.*, vol. 32, no. 6, pp. 1164–1179, Jun. 2014.
- [40] Q. Shi, L. Liu, S. Zhang, and S. Cui, "Device-free sensing in OFDM cellular network," *IEEE J. Sel. Areas Commun.*, vol. 40, no. 6, pp. 1838–1853, Jun. 2022.
- [41] Q. Shi and L. Liu, "Joint LOS identification and data association for 6G-enabled networked device-free sensing," *IEEE Trans. Commun.*, vol. 72, no. 8, pp. 5117–5129, Aug. 2024.
- [42] J. Tang et al., "Cooperative ISAC-empowered low-altitude economy," *IEEE Trans. Wireless Commun.*, vol. 24, no. 5, pp. 3837–3853, May 2025.



Minghao Yuan received the B.S. degree in electronic information engineering from the China University of Geosciences, Beijing, China, in 2018, and the M.S. degree in information and communication engineering from the Beijing Institute of Technology, Beijing, China, in 2022. He is currently pursuing the Ph.D. degree with the School of Information and Electronics, Beijing Institute of Technology. His current research interests include integrated sensing and communication (ISAC), extremely large-scale MIMO, and millimeter-wave communications.



Fan Liu (Senior Member, IEEE) is currently a Professor with the National Mobile Communications Research Laboratory, School of Information Science and Engineering, Southeast University, Nanjing, China. Prior to that, he was an Assistant Professor with the Southern University of Science and Technology, Shenzhen, China, from 2020 to 2024. He received the Ph.D. and the BEng. degrees from Beijing Institute of Technology (BIT), Beijing, China, in 2018 and 2013, respectively. He has previously held academic positions in the University College London (UCL), London, UK, as a Visiting Researcher from 2016 to 2018, and a Marie Curie Research Fellow from 2018 to 2020.

Prof. Liu's research interests lie in the general area of signal processing and wireless communications, and in particular in the area of Integrated Sensing and Communications (ISAC). He is the founding Academic Chair of the IEEE ComSoc ISAC Emerging Technology Initiative (ISAC-ETI), Vice Chair and founding member of the IEEE SPS ISAC Technical Working Group (ISAC-TWG), an elected member of the IEEE SPS Sensor Array and Multichannel Technical Committee (SAM-TC), an Associate Editor of the IEEE Transactions on Communications, IEEE Transactions on Mobile Computing, and IEEE Open Journal of Signal Processing, and a Guest Editor of the IEEE Journal on Selected Areas in Communications, IEEE Wireless Communications, and IEEE Vehicular Technology Magazine. He was a TPC Co-Chair of the 2nd-4th IEEE Joint Communication and Sensing (JC&S) Symposium, a Symposium Co-Chair for the IEEE ICC 2026 and IEEE GLOBECOM 2023, and a Track Co-Chair for the IEEE WCNC 2024. He is a member of the IMT-2030 (6G) ISAC Task Group. He was listed among the World's Top 2% Scientists by Stanford University for citation impact from 2021 to 2024, and among the Elsevier Highly-Cited Chinese Researchers from 2023 to 2024. He was a recipient of numerous Best Paper Awards, including the 2025 IEEE Communications Society & Information Theory Society Joint Paper Award, 2024 IEEE Signal Processing Society Best Paper Award, 2024 IEEE Signal Processing Society Donald G. Fink Overview Paper Award, 2024 IEEE Communications Society Asia-Pacific Outstanding Paper Award, 2023 IEEE Communications Society Stephan O. Rice Prize, and 2021 IEEE Signal Processing Society Young Author Best Paper Award.



Dongxuan He (Member, IEEE) received the B.S. degree in Automation from the Beijing Institute of Technology (BIT) in 2013, and received the Ph.D. degree in Information and Communication Systems from BIT in 2019. From 2017 to 2018, he was a Visiting Student in the Singapore University of Technology and Design (SUTD). From 2019 to 2022, he was a Post-Doctoral Researcher in the Department of Electronic Engineering, Tsinghua University. He is currently an Assistant Professor in the School of Information and Electronics, BIT. His current research interests include Integrated sensing and communication (ISAC), Terahertz communications, and AI empowered wireless communications. He is currently serving as a Guest Editor for the IEEE OPEN JOURNAL OF THE COMMUNICATIONS SOCIETY, the ELECTRONICS, and the SPACE: SCIENCE & TECHNOLOGY. He was a recipient of the Best Paper Award from 2024 IEEE ICSIDP, 2025 IEEE IWCMC. He was also an Exemplary Reviewer of IEEE Wireless Communications Letters.



Hao Yin received the B.S. degree in microwave communication and the M.S. degree in communication and information systems from the Nanjing University of Posts and Telecommunications, Nanjing, China, in 1982 and 1987, respectively, and the Ph.D. degree in communication and information systems from the Beijing Institute of Technology, Beijing, China, in 1999. He is currently an Adjunct Professor with the Army Engineering University of PLA, Nanjing, and a Researcher with the Institute of China Electronic System Engineering, Beijing.

He is a Fellow of the Chinese Academy of Sciences and a Fellow of the China Institute of Communications. His research interests include wireless communication networks and information systems.



Hua Wang (Member, IEEE) received the Ph.D. degree from the Beijing Institute of Technology, Beijing, China, in 1999. From Feb. 2009 to Jan. 2010, he was a Visiting Professor with the Department of Electrical Engineering, Arizona State University, Tempe, AZ, USA. He is currently a Professor with the School of Information and Electronics, Beijing Institute of Technology, Beijing, China. His research interests include communication theory and signal processing, wireless networking, modem design and implementation for satellite communication.



Zhaocheng Wang (Fellow, IEEE) received the B.S., M.S., and Ph.D. degrees from Tsinghua University in 1991, 1993, and 1996, respectively. From 1996 to 1997, he was a Post-Doctoral Fellow with Nanyang Technological University, Singapore. From 1997 to 1999, he was a Research Engineer/Senior Engineer with OKI Techno Centre Pte. Ltd., Singapore. From 1999 to 2009, he was a Senior Engineer/Principal Engineer with Sony Deutschland GmbH, Germany. Since 2009, he has been a Professor with the Department of Electronic Engineering, Tsinghua University, where he is currently the Director of the Broadband Communication Key Laboratory, Beijing National Research Center for Information Science and Technology (BNRist). His research interests include wireless communications, millimeter-wave communications, and optical wireless communications. He was a recipient of the 2016 IEEE Scott Heit Memorial Award, the 2016 IET Premium Award, the 2016 National Award for Science and Technology Progress (First Prize), the ICC2017 Best Paper Award, the 2018 IEEE ComSoc Asia-Pacific Outstanding Paper Award, and the 2020 IEEE ComSoc Leonard G. Abraham Prize.



Tony Q. S. Quek (Fellow, IEEE) received the B.E. and M.E. degrees in electrical and electronics engineering from the Tokyo Institute of Technology in 1998 and 2000, respectively, and the Ph.D. degree in electrical engineering and computer science from the Massachusetts Institute of Technology in 2008. Currently, he is the Cheng Tsang Man Chair Professor with Singapore University of Technology and Design (SUTD) and a ST Engineering Distinguished Professor. He is also the Director of the Future Communications Research and Development Programme, the Head of ISTD Pillar, and the AI on RAN Working Group Chair in AI-RAN Alliance. His current research topics include wireless communications and networking, network intelligence, non-terrestrial networks, open radio access network, and 6G. He is a Fellow of WWRF and the Academy of Engineering Singapore. He was honored with the 2008 Philip Yeo Prize for Outstanding Achievement in Research, the 2012 IEEE William R. Bennett Prize, the 2015 SUTD Outstanding Education Awards-Excellence in Research, the 2016 IEEE Signal Processing Society Young Author Best Paper Award, the 2017 CTTC Early Achievement Award, the 2017 IEEE ComSoc AP Outstanding Paper Award, the 2020 IEEE Communications Society Young Author Best Paper Award, the 2020 IEEE Stephen O. Rice Prize, the 2020 Nokia Visiting Professor, the 2022 IEEE Signal Processing Society Best Paper Award, and the 2024 IIT Bombay International Award For Excellence in Research in Engineering and Technology.